doi:10.1016/j.jmb.2009.01.050 *J. Mol. Biol.* (2009) **387**, 74–91

JMB

Available online at www.sciencedirect.com

ScienceDirect

ELSEVIER

# Sliding Clamp–DNA Interactions Are Required for Viability and Contribute to DNA Polymerase Management in *Escherichia coli*

**Justin M. H. Heltzel[1]†, Sarah K. Scouten Ponticelli[1]†, Laurie H. Sanders[1]†, Jill M. Duzen[1], Vivian Cody[2,3], James Pace[3], Edward H. Snell[2,3] and Mark D. Sutton[1]***

[1]*Department of Biochemistry, School of Medicine and Biomedical Sciences, University at Buffalo, State University of New York, 3435 Main Street, 140 Farber Hall, Buffalo, NY 14214, USA*

[2]*Structural Biology, School of Medicine and Biomedical Sciences, University at Buffalo, State University of New York, Buffalo, NY 14214, USA*

[3]*Hauptman-Woodward Medical Research Institute, Buffalo, NY 14203, USA*

*Received 20 November 2008; accepted 20 January 2009*
Available online
30 January 2009

Sliding clamp proteins topologically encircle DNA and play vital roles in coordinating the actions of various DNA replication, repair, and damage tolerance proteins. At least three distinct surfaces of the *Escherichia coli* β clamp interact physically with the DNA that it topologically encircles. We utilized mutant β clamp proteins bearing G66E and G174A substitutions (β159), affecting the single-stranded DNA-binding region, or poly-Ala substitutions in place of residues 148-HQDVR-152 ($\beta^{148–152}$), affecting the double-stranded DNA binding region, to determine the biological relevance of clamp–DNA interactions. As part of this work, we solved the X-ray crystal structure of $\beta^{148–152}$, which verified that the poly-Ala substitutions failed to significantly alter the tertiary structure of the clamp. Based on functional assays, both β159 and $\beta^{148–152}$ were impaired for loading and retention on a linear primed DNA *in vitro*. In the case of $\beta^{148–152}$, this defect was not due to altered interactions with the DnaX clamp loader, but rather was the result of impaired $\beta^{148–152}$–DNA interactions. Once loaded, $\beta^{148–152}$ was proficient for DNA polymerase III (Pol III) replication *in vitro*. In contrast, $\beta^{148–152}$ was severely impaired for Pol II and Pol IV replication and was similarly impaired for direct physical interactions with these Pols. Despite its ability to support Pol III replication *in vitro*, $\beta^{148–152}$ was unable to support viability of *E. coli*. Nevertheless, physiological levels of $\beta^{148–152}$ expressed from a plasmid efficiently complemented the temperature-sensitive growth phenotype of a strain expressing β159 (*dnaN159*), provided that Pol II and Pol IV were inactivated. Although this strain was impaired for Pol V-dependent mutagenesis, inactivation of Pol II and Pol IV restored the Pol V mutator phenotype. Taken together, these results support a model in which a sophisticated combination of competitive clamp–DNA, clamp–partner, and partner–DNA interactions serve to manage the actions of the different *E. coli* Pols *in vivo*.



*Keywords:* sliding clamp; DNA replication; translesion DNA synthesis; mutagenesis; DNA polymerase

***Edited by M. Gottesman***

**Corresponding author.* E-mail address:mdsutton@buffalo.edu.

Present address: L. H. Sanders, Pittsburgh Institute for Neurodegenerative Diseases, University of Pittsburgh, 3501 5th Avenue, 7th Floor BST3, Room 7045/13B, Pittsburgh, PA 15260, USA.

† These authors contributed equally to this work.

Abbreviations used: Pol, DNA polymerase; TLS, translesion DNA synthesis; SPR, surface plasmon resonance; MMS, methyl methanesulfonate; EDTA, ethylenediaminetetraacetic acid; BSA, bovine serum albumin; RU, response unit.

## Introduction

DNA polymerase III (Pol III) replicates the *Escherichia coli* genome with a remarkably high fidelity.[1] However, endogenous and exogenous agents chronically damage cellular DNA, resulting in lesions that cannot be replicated by Pol III (reviewed in Ref. 2). As a result, faithful duplication of the cell's genetic information requires Pol III as well as a multitude of proteins dedicated to catalyzing DNA repair and DNA damage tolerance (reviewed in Ref. 2). It is generally believed that organisms must tightly regulate the actions of these proteins, in part because many of them compete for the same DNA substrate, and because the Pols involved in potentially error-prone replication over lesions in the DNA, via a process termed translesion DNA synthesis (TLS), display lower fidelities than do replicative enzymes.[3–5] Thus, unregulated access of these proteins to the DNA would lead to mutation and genome rearrangements. Although multiple mechanisms likely contribute to their regulation, one mechanism that has received a large amount of attention in recent years pertains to the role played by sliding clamp proteins. Sliding clamps are well conserved across all three kingdoms of life and are generally believed to play important roles in coordinating protein traffic on DNA by acting as mobile scaffolds. Most partners that bind the clamp do so in part via a conserved clamp-binding motif that inserts itself into a hydrophobic cleft in the clamp.[6] Mutations affecting this clamp-binding motif impair function of the partner protein *in vivo*,[7–10] consistent with clamp acting to manage the actions of these partners *in vivo*. Furthermore, clamps interact with the DNA template that they encircle.[11] Although these clamp–DNA interactions contribute to clamp loading *in vitro*,[11] their importance to viability and Pol management has not yet been established.

In general, *dnaN*-encoded β clamps function as homodimers.[12] The head-to-tail arrangement of the two protomers forms a ring structure with two distinct surfaces. The so-called N-side bears the N-terminus of both protomers, while the C-side contains C-termini as well as two hydrophobic clefts that serve as a common docking site for most of its partner proteins.[6] Sliding clamps are loaded around DNA by a conserved multisubunit $AAA^+$ ATPase referred to as the DnaX clamp loader complex (reviewed in Ref. 13). The minimal functional form of the *E. coli* DnaX complex consists of three copies of any combination of the τ and γ subunits (i.e., $\tau_3$, $\tau_2\gamma_1$, $\tau_1\gamma_2$, or $\gamma_3$), together with one copy each of δ and δ′.[14] Like other clamp loaders, DnaX adopts an arc-shaped structure that is proposed to interact with and stabilize the open form of the β clamp.[15,16] This form of the clamp, in which a single dimer interface is broken, is suggested to adopt a lock washer-like structure.[15] A stable DnaX β clamp complex requires that the τ and/or γ subunits of DnaX first bind ATP (reviewed in Ref. 17). The DnaX–ATP–β complex associates with the 3′ end of either nicked or primed DNA. Once properly positioned, the DnaX complex hydrolyzes bound ATP, resulting in its rapid dissociation, leaving the clamp behind to assemble on DNA. Recently, the O'Donnell, Kong, and Kuriyan laboratories described the X-ray crystal structure of the β clamp assembled on a short primed DNA template.[11] In the crystal, specific contacts between the clamp and both single-stranded (ss) and double-stranded (ds) regions of the DNA template were observed.[11] Furthermore, several amino substitutions targeting residues predicted to be involved in clamp–DNA interactions served to reduce the efficiency with which the clamp was loaded onto DNA *in vitro*.[11] These clamp–DNA interactions were also suggested to contribute to Pol switching as part of a toolbelt model,[11] which states that two different Pols are bound to the same clamp, with each Pol contacting the cleft of a different clamp protomer.[18] The DNA template passes through the clamp at a 22° angle relative to the N- and C-sides of the clamp, which serves to place one of the two clefts of β in closer proximity to the 3′-OH of the primer. In the context of the toolbelt model, Pol switching may involve the clamp acting like a toggle switch, effectively removing one Pol from the primer/template end while simultaneously enabling access of a second Pol.[11] This toggling may be mediated in part by clamp–DNA interactions. However, neither this provocative model nor the biological relevance of the clamp–DNA interactions was investigated.

The purpose of the work discussed in this report was to establish the biological role(s) of clamp–DNA interactions in *E. coli*. We focused largely on the

**Fig. 1.** X-ray crystal structure of the mutant $\beta^{148-152}$ clamp protein. (a) Face view (C-side) of the structure of the mutant $\beta^{148-152}$ clamp protein depicted in ribbon form. The three subdomains composing each protomer (A1-3 and B1-3) are indicated, as are the positions of the loops containing the 148-HQDVR-152 poly-Ala substitutions (150; depicted as space-filled atoms) and residues L21–L27 (24; depicted in ribbon form). Protomer A is in green, and protomer B is in blue. (b) Face view (C-side) of the wild-type β clamp protein (purple) encircling primed DNA, the backbone of which is shown in gold (PDB code 3BEP).[11] Protomer A of $\beta^{148-152}$ from (a) (green) is superimposed onto protomer A of the wild-type clamp (purple). Positions of the 148-HQDVR-152 poly-Ala substitutions, G66 and G174, which are substituted with E and G, respectively, in β159, as well as P20, which is substituted with L in *dnaN783* and acts to suppress the temperature-sensitive growth phenotype of the *dnaN159* allele,[20] are indicated. Enlarged views of the loop containing residues 148-HQDVR-152 in protomer A (c) or B (d) are shown. Wild-type β (PDB code 1OK7)[21] is depicted in green, while $\beta^{148-152}$ is in yellow (c) or purple (d). (e) Enlarged view of the loop containing residues L21–L27. Protomer A of wild-type β (PDB code 1OK7) is depicted in yellow, while protomer A of $\beta^{148-152}$ is in green. (f) Enlarged view of the water network near the $\beta^{148-152}$ dimer interface. Positions R269 of protomer A (yellow) and S101 and S104 of protomer B (purple) are indicated. Water is depicted as space-filled atoms. (g) Enlarged view of the interaction of protomer A of $\beta^{148-152}$ with calcium present in the crystallization buffer. Positions of resides E52, N118, and L119 are indicated. Calcium is depicted as space-filled atoms.

mutant $\beta^{148–152}$ clamp protein for this work, since residues H148 and Q149 of the clamp interact directly with the DNA template but do not appear to interact with DnaX or Pol III.[11,19] In addition, this mutant protein was impaired for Pol V mutagenesis,[19] suggesting that detailed characterization of $\beta^{148–152}$ would help to define the extent to which clamp–DNA interactions influenced Pol usage *in vivo*. This project was initiated by solving the X-ray crystal structure of the dimeric $\beta^{148–152}$ clamp mutant. Our structure verified that the poly-Ala substitutions failed to significantly alter the tertiary structure of the clamp protein. Based on functional assays, loading of $\beta^{148–152}$ onto a primed DNA template was impaired, despite its ability to interact normally with DnaX. Although $\beta^{148–152}$ was proficient for stimulating Pol III replication *in vitro*, it was severely impaired for stimulating Pol II and Pol IV replication. Moreover, $\beta^{148–152}$ was unable to support viability of *E. coli*. Nevertheless, physiological

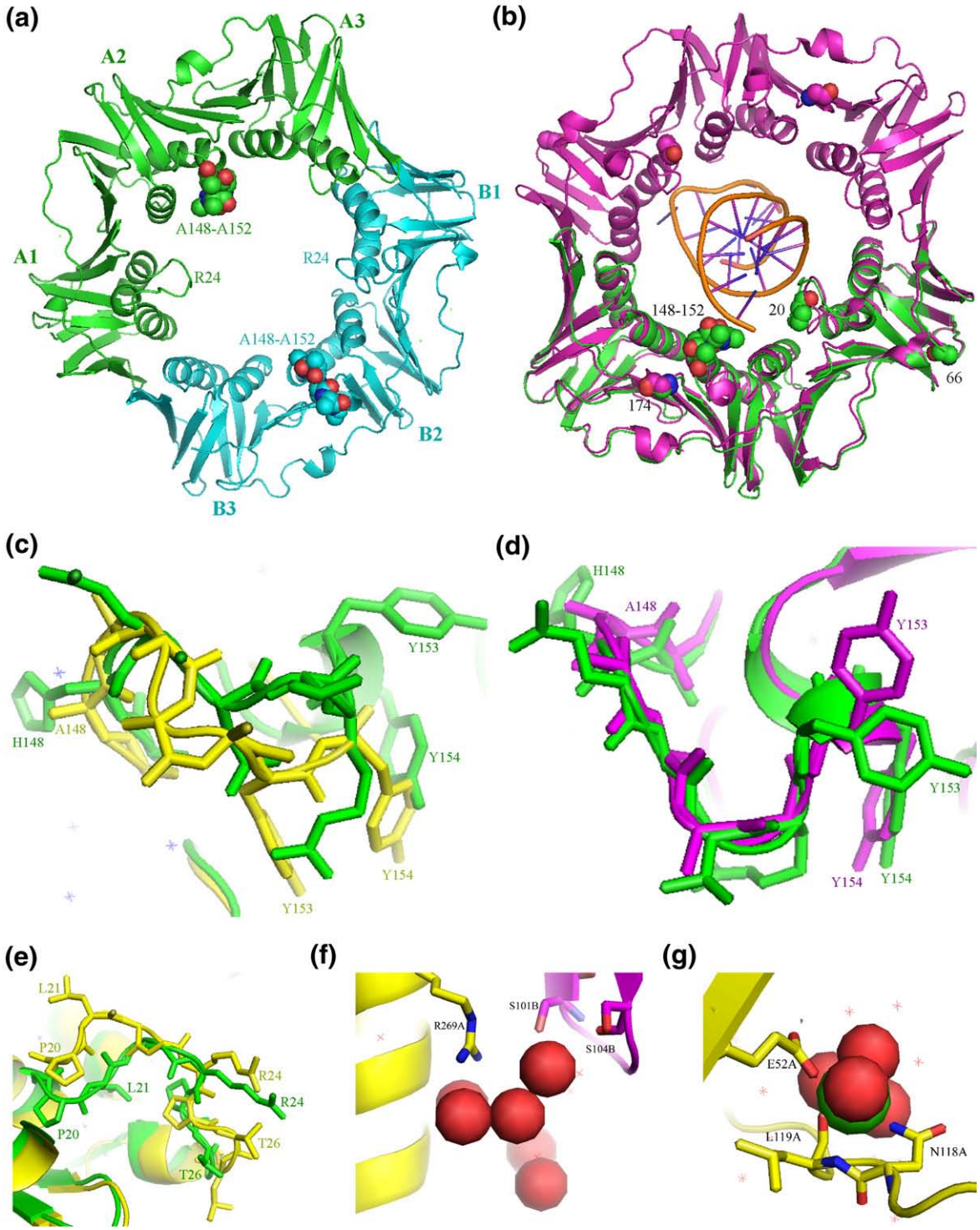


**Fig. 1** *(legend on previous page)*

levels of $\beta^{148–152}$ expressed from a plasmid fully complemented the temperature-sensitive growth phenotype of the *dnaN159* (β159) strain, provided that Pol II and Pol IV were inactivated. The β159 mutant was impaired for loading and retention on a linear DNA, arguing that complementation was most likely due to the formation of a β159–$\beta^{148–152}$ heterodimer. Furthermore, Pol V-dependent mutagenesis was restored in the *dnaN159* strain expressing $\beta^{148–152}$ when both Pol II and Pol IV were inactivated. Taken together, these results support a model in which the sophisticated coordination of competitive clamp–partner, clamp–DNA, and partner–DNA interactions serve to manage the actions of the various *E. coli* Pols *in vivo*. Our findings are discussed in terms of models for coordination of replication, repair, and TLS.

## Results

### Structure of the mutant $\beta^{148–152}$ sliding clamp protein

Residues 148-HQDVR-152 of the *E. coli* β clamp are within a large solvent-exposed loop that interacts with DNA on the C-side near the cleft (Fig. 1). To determine whether substitution of these residues with poly-Ala ($\beta^{148–152}$) altered the tertiary structure of the clamp, we solved the X-ray crystal structure of $\beta^{148–152}$ (Table 1). As summarized in Fig. 1, the structure of $\beta^{148–152}$ and those previously reported for the wild-type clamp were remarkably similar.[12,21,22] An overlay of the α-carbon backbones of our $\beta^{148–152}$ structure with that of the wild-type clamp revealed an RMSD of only 0.71 Å. Each clamp protomer is composed of three ~110-residue subdomains containing an identical chain topology with pseudo 2-fold symmetry composed of a scaffold of two β sheets that encompass two α helices (Fig. 1a).[12] The primary structural effect of the substitution of residues 148-HQDVR-152 with poly-Ala in $\beta^{148–152}$ is observed in protomer A (Fig. 1c), with this effect restricted almost entirely to the poly-Ala substitution. In protomer A of $\beta^{148–152}$, the α-carbon atoms of Y153 and Y154, which stack with nucleotide bases in the template DNA, were moved 6.55 and 5.22 Å, respectively, relative to these same positions in $\beta^{+}$ (Fig. 1c).[12,22] In contrast, the conformation of this loop in protomer B was similar to that of the wild-type clamp, and the α-carbon atoms of Y153 and Y154 were moved only 0.7 and 0.82 Å, respectively, compared to $\beta^{+}$ (Fig. 1d).

Three additional structural features of the $\beta^{148–152}$ mutant differed from the wild-type β sliding clamp structures previously reported, including (i) the conformation of the loop region encompassing residues L21 to L27 (Fig. 1e), which interacts with dsDNA[11] and is relatively flexible;[22] (ii) the observation of a tight hydrogen-bonding network of water molecules near the dimer interface involving residue R269 in protomer A and S101 and S104 of protomer B, each of which is near the homodimer interface (Fig. 1f);[23] and (iii) the presence of a calcium ion from the crystallization buffer (Fig. 1g). The calcium makes octahedral coordination to the backbone carbonyl of L119 and the side chain of N118 in both protomers and to water molecules that form an extended secondary hydrogen-bonding network. These differences are likely to be independent of the poly-Ala substitutions. Thus, we conclude that substitution of residues 148-HQDVR-152 in $\beta^{148–152}$ with poly-Ala serves to remove amino acid side chains involved in direct interaction with the DNA template (Fig. 1b) and additionally alters the positions of Y153 and Y154 that stack with template DNA bases without significantly affecting the overall tertiary structure of the protein.

**Table 1.** Crystallographic data for *E. coli* $\beta^{148–152}$ mutant sliding clamp

| | |
|---|---|
| Beamline | SSRL |
| Wavelength (Å) | 1.000 |
| Resolution (Å) | 28.855–1.767 |
| Space group | *P*1 |
| Temperature (K) | 100 |
| Detector | Mar325 CCD |
| Unit cell parameters | *a*=40.838 Å, *b*=64.471 Å, *c*=72.111 Å α=73.83°, β=82.72°, γ=83.76° |
| Solvent content (%) | 43.87 |
| Unique reflections | 59,193 |
| $I/\sigma(I)$ | 23.3 (2.03)[a] |
| Average redundancy | 1.8 (1.6) |
| Data completeness (%) | 91.8 (80.8) |
| Mosaicity (%) | 2.0 |
| $R_{merge}$ (%) | 0.035 (0.347) |
| Refinement: | |
| *R* factor (%) | 21.8 |
| $R_{free}$ (%)[b] | 28.3 |
| RMSD bond distance (Å) | 0.019 |
| RMSD bond angle (°) | 2.08 |
| Average *B*-factors (Å$^2$) | 35.3 |
| Ramachandran plot | |
| Core (%) | 90.3 |
| Disallowed (%) | 0.8 |
| No. of protein atoms | 5648 |
| No. of solvent atoms | 381 |
| PDB code | 3F1V |

[a] Values in parentheses refer to the highest-resolution shell, 1.83–1.77 Å.
[b] $R_{free}$ is calculated the same way as *R* factor for data omitted from refinement (5% of reflections for all data).

### The mutant $\beta^{148–152}$ clamp protein is proficient for interaction with the DnaX complex, but is nevertheless severely impaired for loading onto primed DNA *in vitro*

The DnaX clamp loader complex interacts with β largely through association of residues L73–F74 of the δ subunit of DnaX with the hydrophobic cleft of the clamp.[24] Since the tertiary structure of the cleft region of $\beta^{148–152}$ was unaffected by the poly-Ala substitutions (Fig. 1a), we presumed that this mutant clamp would interact normally with DnaX. As a direct test of this hypothesis, we used surface

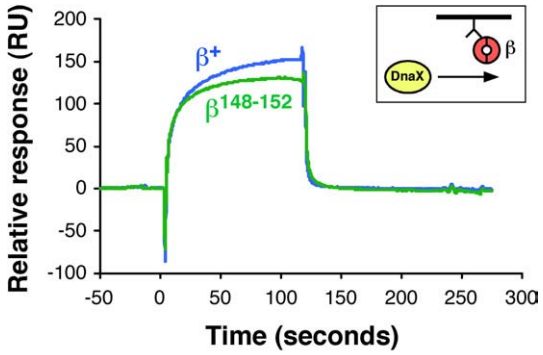


| β clamp | $K_D$ (nM) | $k_a$ ($M^{-1}s^{-1}$) | $k_d$ ($s^{-1}$) |
|---|---|---|---|
| $\beta^+$ | 27 | $7.84 \times 10^6$ | 0.2 |
| $\beta^{148-152}$ | 43 | $4.86 \times 10^6$ | 0.2 |

**Fig. 2.** Interactions of $\beta^+$ and $\beta^{148-152}$ with the DnaX clamp loader complex. The top panel shows representative SPR results with injection of 25 nM DnaX complex ($\gamma_3\delta\delta'\chi\psi$) over ~100 RU of $\beta^+$ or $\beta^{148-152}$ captured on the chip surface. The approach is described in Material and Methods and is summarized in cartoon form in the inset. The table at the bottom summarizes kinetic values describing the interactions. Values were obtained by injection of 0, 1, 10, 50, 100, 200, or 400 nM DnaX over ~100 RU of $\beta^+$ or $\beta^{148-152}$.

plasmon resonance (SPR) to measure clamp–DnaX interactions. Briefly, anti-Penta-His antibody covalently attached to the surface of the sensor chip was used to capture N-terminally $His_6$-tagged forms of $\beta^+$ or $\beta^{148-152}$. To determine affinities of $\beta^+$ and $\beta^{148-152}$ for the clamp loader, different concentrations of DnaX ranging from 1 to 400 nM were preincubated with ATP and injected over the chip surface. A typical result using ~100 response units (RU) clamp and 25 nM DnaX is shown in Fig. 2. Analysis of the complete data sets revealed that $\beta^+$ and $\beta^{148-152}$ had similar affinities for DnaX (27 and 43 nM, respectively). Thus, we conclude that residues H148–R152 of the clamp do not contribute significantly to interactions with DnaX.

We next measured the efficiency by which $\beta^+$ and $\beta^{148-152}$ were loaded onto a primed DNA, again using an SPR-based assay. This assay was described previously[25] and monitors loading of the clamp onto a linear 30/80-mer primer/template DNA that is tethered to the streptavidin chip surface via a 3′-biotin tag (Fig. 3a). Injection of DnaX–ATP complex over the chip surface led to an increase in RU due to DnaX–DNA interactions (Fig. 3b). This signal returned to baseline almost immediately upon washing of the chip surface with the clamp-loading buffer due to the rapid dissociation of DnaX from the DNA.[25] Injection of DnaX–ATP–$\beta^+$ complex led to a more robust RU signal than did DnaX–ATP alone, which increased steadily with time, reflecting loading of clamp onto the DNA template (Fig. 3b).

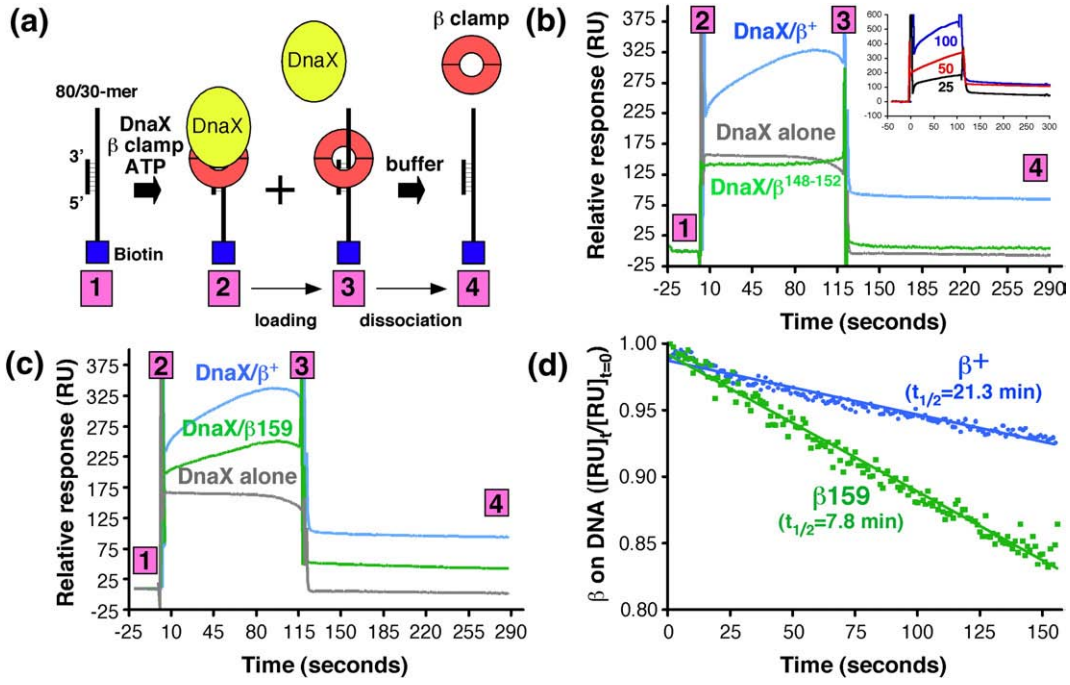


**Fig. 3.** Ability of DnaX to load wild-type or mutant clamps onto a linear primed DNA template. (a) The approach used for measuring clamp loading and retention of the clamp on DNA is depicted in cartoon form. Clamp loading reactions contained 50 nM DnaX complex and 250 nM (as dimer) of $\beta^+$ or $\beta^{148-152}$ (b) or $\beta^+$ and β159 (c) in HBS-EP buffer lacking EDTA and supplemented with 1 mM ATP and 10 mM $MgCl_2$. The level of DnaX used was determined experimentally based on a titration of DnaX [25 (black), 50 (red), or 100 nM (blue)] using a fixed level of $\beta^+$ (250 nM), as shown in the inset to (b). (d) The half-life for the stability of clamp on DNA was measured by plotting the change in RU signal as a function of time. Half-life was measured using results contained between step 3 and step 4 of the results shown in (b) and (c).

The magnitude of this signal was directly proportional to the level of DnaX used, indicating that clamp loader was limiting under these conditions (Fig. 3b, inset). Furthermore, a significant portion of this signal persisted even after the buffer wash, despite the fact that the template was linear, due to clamp–DNA interactions (Fig. 3b). Thus, this assay simultaneously measures both clamp loading and clamp–DNA interactions. Based on regression analysis (Fig. 3d), the wild-type β clamp had a half-life on the linear DNA of ~21.3 min. This value represents the time it takes for the clamp to slide off the free single-stranded 5′ end of the DNA template (Fig. 3a).

We next examined loading of $\beta^{148–152}$ with the same approach. As summarized in Fig. 3b, $\beta^{148–152}$ failed to accumulate on the DNA template. Based on the shape of the SPR signal, it appeared that the DnaX–ATP–$\beta^{148–152}$ complex was able to bind to the DNA template and was loaded, albeit inefficiently. However, we were unable to extrapolate a half-life for the $\beta^{148–152}$–DNA complex due to the low level of clamp retained on the DNA. As discussed below, $\beta^{148–152}$ was loaded onto a circular primed DNA template, as measured by Pol III replication, provided sufficient time was granted (Fig. 4). Thus, we interpret the inefficient loading observed with the SPR assay (Fig. 3b) to be the result of both a loading defect and a rapid dissociation of the $\beta^{148–152}$ mutant clamp off the free 5′ end of the template DNA. Taken together, these findings indicate that $\beta^{148–152}$ interacts normally with DnaX complex, but is nonetheless severely impaired for loading onto a linear primed DNA template, presumably due to impaired clamp–dsDNA interactions.[11]

## The mutant $\beta^{148–152}$ clamp protein is proficient for Pol III replication, but is severely impaired for Pol II and Pol IV replication *in vitro*

We next asked whether $\beta^{148–152}$ was proficient for stimulating Pol III replication *in vitro*. We first measured the ability of $\beta^{+}$ or $\beta^{148–152}$ to stimulate replication by Pol III*. Pol III* is composed of one DnaX complex in association with two Pol III cores, which are responsible for DNA polymerization and proofreading functions, but lacks β clamp. Replication activity was measured by quantitating incorporation of [$^{3}$H]deoxythymidine triphosphate (dTTP) with the use of liquid scintillation spectroscopy, as described previously.[20,26] Although $\beta^{+}$ stimulated Pol III* replication robustly, $\beta^{148–152}$ was only marginally better than control reactions without β clamp (Fig. 4a). Using a staged assay, we next measured replication, in which we preincubated $\beta^{+}$ or $\beta^{148–152}$ with the DNA template, DnaX, and ATP for 5 min to permit loading of the clamp prior to the addition of Pol III core. Under these conditions, $\beta^{148–152}$ was proficient in stimulating Pol III replication, and total nucleotide incorporation approached the level observed for the wild-type clamp (Fig. 4b). More importantly, these results also indicate that the inefficient loading observed with the SPR assay discussed above was due, in large part, to the inability of $\beta^{148–152}$ to remain

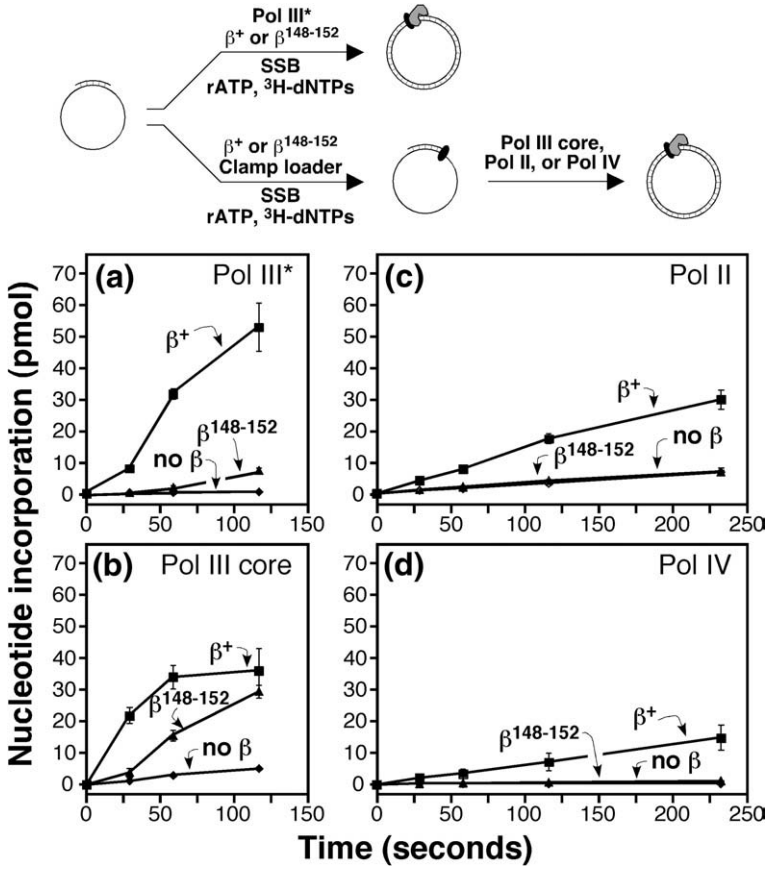


**Fig. 4.** Ability of $\beta^{148–152}$ to stimulate processivity of Pol III, Pol II, and Pol IV. The ability of $\beta^{+}$ or $\beta^{148–152}$ to stimulate replication by Pol III* (a), Pol III core (b), Pol II (c), or Pol IV (d) was measured as described in Materials and Methods. Clamp loading and replication were either concurrent, as for Pol III* (a), or staged 5 min, as for Pol III core (b), Pol II (c), and Pol IV (d), as summarized in the cartoon at the top of the figure. The $\tau_2\gamma_1\delta\delta'\chi\psi$ form of the DnaX complex was used with Pol III core, while $\gamma_3\delta\delta'$ was used with Pol II and Pol IV. Results shown represent the average of at least three independent determinations. Error bars represent the standard deviation.

associated with a linear DNA template (Fig. 3c). Taken together, results discussed in Figs. 3 and 4 confirm that $\beta^{148–152}$ was primarily impaired for clamp loading due to impaired clamp–DNA interactions, but once loaded, was largely proficient for supporting Pol III replication *in vitro*.

In addition to Pol III, we also analyzed the ability of $\beta^{148–152}$ to stimulate replication of Pol II and Pol IV *in vitro*. To compensate for the loading defect of the $\beta^{148–152}$ mutant clamp (Fig. 3b), we preincubated the primed M13 DNA template with the DnaX–ATP complex and either $\beta^+$ or the $\beta^{148–152}$ mutant clamp for 5 min prior to the addition of Pol II or Pol IV. In striking contrast to the wild-type clamp, which stimulated replication of both Pol II and Pol IV, $\beta^{148–152}$ did not stimulate replication of either Pol (Fig. 4c and d). Consistent with these findings, $\beta^{148–152}$ was impaired for direct physical interaction with both Pol II and Pol IV, albeit to different degrees (Table 2). Taken together, these results indicate that residues H148–R152 of the clamp are dispensable for Pol III replication after the clamp is loaded, but are required for functional interactions with Pol II and Pol IV.

## The $\beta^{148–152}$ mutant does not support viability of *E. coli*

To determine whether β clamp–DNA interactions are essential for clamp function *in vivo*, we asked whether $\beta^{148–152}$ could support viability of *E. coli*. For this, we utilized a method described by Datsenko and Wanner[27] to replace the *dnaN*$^+$ allele with *dnaN*$^{148–152}$, which encodes $\beta^{148–152}$. Briefly, this method involves electroporation of a strain expressing the λ Red recombination function with a PCR fragment encoding the sequence to be crossed onto the chromosome. To provide a positive selection for crossover products, we cloned a recombinant cassette containing the tetracycline resistance (*tet*) gene between the *dnaN* and *recF* loci (Fig. 5a). In addition, we also introduced a silent mutation that disrupts a PvuII site in *dnaN*$^{148–152}$ to facilitate detection of the allele (Fig. 5a). Following selection for Tet$^R$, we used a diagnostic PCR assay to verify that the *dnaN*$^+$*-tet* cassette was inserted between the *dnaA* and *recF* genes (Fig. 5b). We first asked whether we could cross the *dnaN*$^{148–152}$ allele onto the chromosome of *E. coli* strain AB1157. Although we were able to consistently cross the *dnaA-dnaN*$^+$*-tet-recF* cassette onto the AB1157 chromosome (Fig. 5b), we were unable to recombine a similar cassette bearing *dnaN*$^{148–152}$. We therefore constructed an *E. coli* strain bearing an ectopic N-terminally His$_6$-tagged copy of the *dnaN*$^+$ allele within the *lamB* gene, referred to as *lamB*::(His$_6$-*dnaN*$^+$*-cat*) (Fig. 5c). We hypothesized that expression of the His$_6$-tagged $\beta^+$ protein from this ectopic allele would support viability of the strain irrespective of what we replaced the endogenous *dnaN* locus with. As summarized in Fig. 5b, we were able to cross both the *dnaA-dnaN*$^+$*-tet-recF* and *dnaA-dnaN*$^{148–152}$*-tet-recF* cassettes onto the chromosome of the *lamB*::(His$_6$-*dnaN*$^+$*-cat*) strain. However, as discussed below (see Fig. 6), growth of the $\beta^{148–152}$ strain was dependent on an ectopic *dnaN*$^+$ allele, indicating that $\beta^{148–152}$ was unable to support viability of *E. coli* strain AB1157.

## $\beta^{148–152}$ can complement the temperature-sensitive growth phenotype of the *dnaN159* strain, provided that Pol II and Pol IV are inactivated

Our finding that $\beta^{148–152}$ failed to support viability of *E. coli* AB1157 contrasts with our finding that physiological levels of $\beta^{148–152}$ expressed from a plasmid complemented the temperature-sensitive growth phenotype of an AB1157 derivative bearing the *dnaN159* allele at the nonpermissive temperature of 37 °C.[19] One likely explanation for these results is that $\beta^{148–152}$ complements the *dnaN159* strain through formation of a temperature-resistant β159–$\beta^{148–152}$ heterodimer. Since Pol IV enhanced the temperature-sensitive growth phenotype of the *dnaN159* strain,[28–30] and $\beta^{148–152}$ was unable to stimulate Pol IV replication *in vitro* (Fig. 4d), we reasoned that if growth of the *dnaN159* strain bearing the $\beta^{148–152}$-expressing plasmid at the elevated temperature was dependent on a temperature-resistant β159–$\beta^{148–152}$ heterodimeric clamp protein, then inactivation of Pol IV would increase the temperature at which this strain was able to grow. Likewise, Pol II and Pol V are also able to impair growth of the *dnaN159* strain under constitutive SOS-induced conditions,[29,30] and as such, these Pols might similarly impair growth of the *dnaN159* strain bearing the $\beta^{148–152}$-expressing plasmid. We therefore asked whether inactivation

**Table 2.** Affinity of $\beta^+$ and $\beta^{148–152}$ for Pol II and Pol IV

| DNA polymerase | β clamp protein | $K_D$ (nM) | $k_a$ ($M^{-1}$ $s^{-1}$) | $k_d$ ($s^{-1}$) | $\chi^2$ value[a] |
|---|---|---|---|---|---|
| Pol II | $\beta^+$ | 31.6 | $3.77\times10^4$ | $1.19\times10^{-3}$ | 3.3 |
| | $\beta^{148–152}$ | 182 | $1.51\times10^4$ | $2.73\times10^{-3}$ | 3.9 |
| Pol IV | $\beta^+$ | 465 | $1.53\times10^4$ | $7.13\times10^{-3}$ | 10.7 |
| | $\beta^{148–152}$ | 680 | $2.42\times10^4$ | $3.04\times10^{-3}$ | 4.9 |

Interactions were measured by SPR using a BIAcore X instrument as described in Materials and Methods. For Pol II, ~250 RU of the N-terminally His$_6$- and kinase-tagged forms of $\beta^+$ or $\beta^{148–152}$ was captured on the chip surface using anti-Penta-His antibody (Qiagen), and Pol II was injected over a concentration range of 1 nM to 2.5 μM. For Pol IV, ~500 RU of $\beta^+$ or $\beta^{148–152}$ was captured on the chip surface, and Pol IV was injected over a concentration range of 15 nM to 1.5 μM.

[a] The $\chi^2$ value describes the fit of the raw data to the 1:1 Langmuir model used for determination of kinetic values and was derived with the BIAevaluation software.

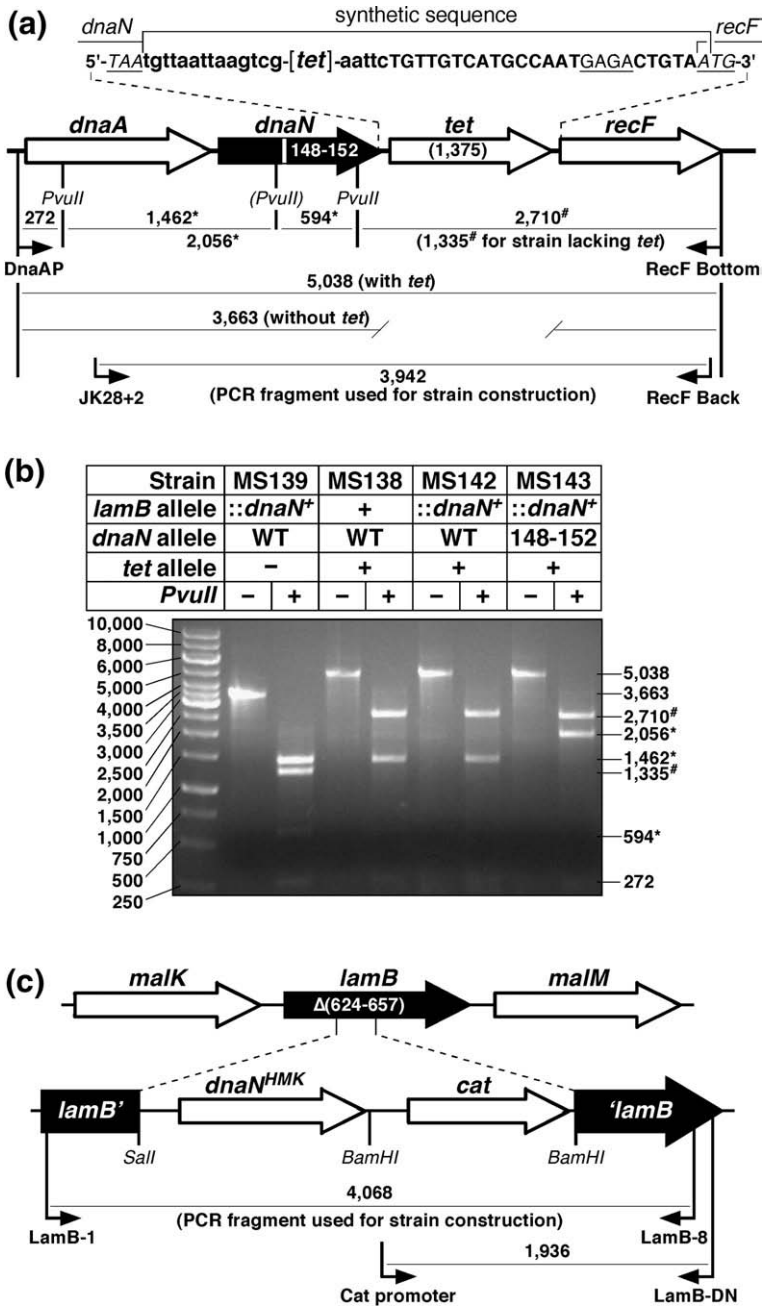


**Fig. 5.** Construction of tagged *dnaN*$^{+}$ and *dnaN*$^{148–152}$ *E. coli* strains. (a) Physical map of the *dnaA* operon depicting the structure of the *dnaA-dnaN*$^{+}$*-tet-recF* and *dnaA-dnaN*$^{148–152}$*-tet-recF* alleles. The specific DNA sequence flanking the *tet* gene is indicated. Nucleotide sequence depicted in lower case flanking the *tet* coding sequence ([*tet*]) was inserted as part of the *tet* cassette as described in Materials and Methods. The Shine–Delgarno sequence for *recF* is underlined, and the stop (*TAA*) and start (*ATG*) codons for *dnaN* and *recF*, respectively, are indicated. The PvuII restriction site that is disrupted in the *dnaN*$^{148–152}$ allele is indicated by parentheses. Predicted sizes of PvuII restriction fragments for the *dnaA-dnaN*$^{+}$*-tet-recF* and *dnaA-dnaN*$^{148–152}$*-tet-recF* alleles are indicated. (b) Representative results from PvuII restriction digestion of the PCR-amplified *dnaA* operon region from *dnaN*$^{+}$ *lamB*: :(His$_6$-*dnaN*$^{+}$-*cat*) (MS139), *dnaA-dnaN*$^{+}$*-tet-recF* (MS138), *dnaA-dnaN*$^{+}$*-tet-recF lamB*: :(His$_6$-*dnaN*$^{+}$-*cat*) (MS142), and *dnaA-dnaN*$^{148–152}$*-tet-recF lamB*: :(His$_6$-*dnaN*$^{+}$-*cat*) (MS143) strains are shown. The asterisk denotes those fragments resulting from the loss of the PvuII restriction site in *dnaN*$^{148–152}$. The number sign denotes those fragments resulting from insertion of the *tet* cassette between *dnaN* and *recF*. (c) Physical map of the *lamB* locus depicting the structure of the *lamB*: :(His$_6$-*dnaN*$^{+}$-*cat*) cassette. Primers used for strain construction or for diagnostic PCR to confirm the structure of the insertion in strain MS139 as well as sizes for respective PCR products are shown.

of Pol II (Δ*polB*: :Ω), Pol IV [Δ(*dinB-yafN*): :*kan*], or Pol V (Δ*umuDC595*: :*cat*) improved the ability of $\beta^{148–152}$ to complement the temperature-sensitive growth phenotype of the *dnaN159* strain. As summarized in Table 3, inactivation of Pol II severely impaired growth of the *dnaN159* strain expressing $\beta^{148–152}$ at both 30 and 42 °C. Moreover, inactivation of either Pol IV or Pol V failed to suppress temperature-sensitive growth of the *dnaN159* strain expressing $\beta^{148–152}$ (Table 3).

Since Pol usage is altered in the *dnaN159* strain,[20,28] we next asked whether $\beta^{148–152}$ could complement growth at 42 °C of a *dnaN159* strain lacking all possible combinations of these three Pols. Although the $\beta^{148–152}$ mutant was unable to complement temperature-sensitive growth of the Pol II–Pol V- and Pol IV–Pol V-deficient mutants, it was able to fully complement temperature-sensitive growth of the Pol II–Pol IV mutant (Table 3). Further inactivation of Pol V in the Pol II–Pol IV mutant failed to improve growth of the $\beta^{148–152}$-expressing strain (Table 3). Taken together, these findings (i) indicate that Pol IV was responsible for the poor growth phenotype of the *dnaN159* Pol II-deficient strain expressing the $\beta^{148–152}$ mutant (Table 3), presumably through contact of these Pols with β159, and (ii) support the model that $\beta^{148–152}$ and β159 form a heterodimeric clamp capable of supporting temperature-resistant growth of *E. coli*.

In light of these results (Table 3), we asked whether $\beta^{148–152}$ could support viability of an *E. coli* strain lacking Pol II and Pol IV. For this, we used

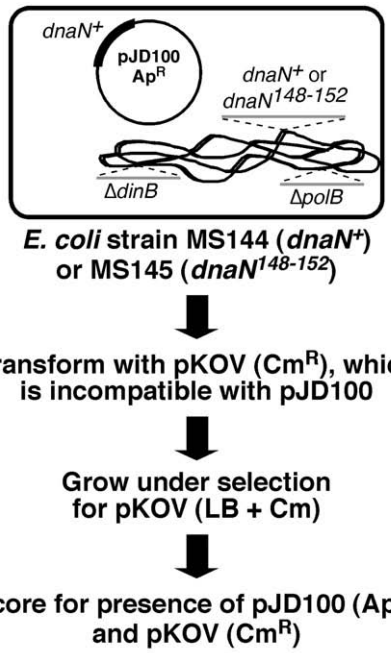


| Strain | *dnaN* allele | Ratio of CFU bearing pJD100 ($Ap^R$)/pKOV ($Cm^R$) | | |
|---|---|---|---|---|
| | | Exp | $Ap^R/Cm^R$ | Total |
| MS144 | *dnaN+* | 1 | 0/34 | |
| | | 2 | 3/41 | |
| | | 3 | 0/43 | 3/118 |
| MS145 | *dnaN148-152* | 1 | 41/41 | |
| | | 2 | 38/38 | |
| | | 3 | 38/38 | 117/117 |

**Fig. 6.** The *dnaN*$^{148–152}$ (β$^{148–152}$) allele does not support viability of *E. coli*. Cartoon depicting the plasmid shuffle assay used to assess viability of *dnaA-dnaN*$^+$*-tet-recF* (MS144) and *dnaA-dnaN*$^{148–152}$*-tet-recF* (MS145) strains bearing the *dnaN*$^+$-expressing plasmid pJD100 is shown above. Results from three independent plasmid shuffle experiments with strains MS144 and MS145 are summarized below in the table.

phage P1*vir* to transduce the *dnaN*$^{148–152}$*-tet* or *dnaN*$^+$*-tet* cassette from the respective merodiploids bearing the *lamB*::(His$_6$-*dnaN*$^+$*-cat*) allele into a strain that was deficient for both Pol II and Pol IV, lacked the ectopic *lamB*::(His$_6$-*dnaN*$^+$*-cat*) allele (Fig. 5b), and contained the low-copy-number plasmid pJD100 that expresses physiological levels of *dnaN*$^+$.[19,28] We then asked whether viability of this strain was dependent on the plasmid-expressed β$^+$ clamp using a plasmid shuffle approach (see Fig. 6). As summarized in Fig. 6, we were unable to cure the *dnaN*$^{148–152}$ strain of the β$^+$-expressing plasmid. In contrast, we were able to efficiently cure this plasmid from the isogenic *dnaN*$^+$ strain (Fig. 6). These results indicate that the inability of β$^{148–152}$ to support viability of *E. coli* was independent of Pol II and Pol IV and further support the model that clamp–DNA interactions are essential for proper clamp function *in vivo*.

## The mutant β159 clamp is partially impaired for both loading and clamp–DNA interactions

We hypothesized that viability of *E. coli* may not require that both subunits of the clamp contact DNA in the same way. Consistent with this hypothesis, the G174A substitution of β159 resides in the hydrophobic cleft, which interacts with ssDNA, whereas residues H148 and G149, which are substituted with A in β$^{148–152}$, mediate interaction with dsDNA.[11] We were therefore interested in determining whether β159 was impaired for loading and retention on a linear DNA using the SPR loading assay described above (see Fig. 3a). DnaX loaded β159 onto DNA, albeit less efficiently than did β$^+$ (Fig. 3; compare b and c). Once loaded, β159 remained on the DNA with a half-life of ~7.8 min, compared to ~21.3 min for β$^+$ (Fig. 3d). These results support a model in which the β159–β$^{148–152}$ heterodimer supports viability of *E. coli* because its two subunits are impaired for DNA interactions in different ways. An effort was made to purify a β159–β$^{148–152}$ heterodimer for *in vitro* characterization; however, we have not yet succeeded in purifying this heterodimeric clamp to homogeneity.

## Inactivation of both Pol II and Pol IV restores Pol V-dependent DNA-damage-induced mutagenesis in the *dnaN159* strain expressing physiological levels of β$^{148–152}$

We previously demonstrated that the *dnaN159* strain expressing the β$^{148–152}$ mutant was severely impaired for Pol V-dependent mutagenesis following UV irradiation (Fig. 7a).[19] Since inactivation of Pol II and Pol IV improved growth of the *dnaN159* strain expressing β$^{148–152}$ (Table 3), we asked whether inactivation of these Pols restored Pol V-dependent mutagenesis in the β$^{148–152}$-expressing strain. We were unable to measure the effect on mutagenesis of inactivation of Pol II alone due to the poor growth phenotype of the Pol II-deficient strain expressing β$^{148–152}$ (Table 3). Consistent with our previous observations,[19] the *dnaN159* strain expressing β$^+$ was proficient for UV-induced mutagenesis at 37 °C, while the same strain expressing β$^{148–152}$ was severely impaired (Fig. 7a). Inactivation of Pol IV had only a modest effect on mutation frequency of the *dnaN159* strain expressing β$^+$ or β$^{148–152}$ (Fig. 7a). In contrast, inactivation of both Pol II and Pol IV restored a robust UV-induced mutator phenotype in the β$^{148–152}$-expresing strain at both 37 (Fig. 7a) and 42 °C without significantly affecting the frequency in the β$^+$ control. As a control, Pol V was also inactivated, which abrogated UV-induced mutagenesis, thus verifying its Pol V dependence (Fig. 7a).

As part of these studies, we also analyzed Pol V-dependent methyl methanesulfonate (MMS)-induced mutagenesis.[37] We first compared the efficiency of MMS-induced mutagenesis using isogenic *dnaN*$^+$ and *dnaN159* strains. For these experiments, we focused on strains MS100 (*dnaN*$^+$) and MS101 (*dnaN159*), because this *dnaN159* mutant is

**Table 3.** Ability of $\beta^+$ and $\beta^{148–152}$ to complement the tem8perature-sensitive growth phenotype of various *dnaN159* mutant strains deficient in specialized Pols

| | Relevant genotype[b] | | | Ratio (42 °C/30 °C) of colony-forming units/ml for *dnaN159* strain transformed with[c] | | |
|---|---|---|---|---|---|---|
| *E. coli* strain[a] | *polB* | *dinB* | *umuDC* | Control plasmid | *dnaN*$^+$ | *dnaN*$^{148–152}$ |
| MS120 | + | + | + | $<(4.2\pm1.1)\times10^{-5}$ | $1.1\pm0.09$ | $(0.67\pm0.53)\times10^{-3}$ |
| MS134[d] | Δ | + | + | $(0.73\pm0.45)\times10^{-5}$ | $0.93\pm0.09$ | $(0.66\pm0.49)\times10^{-1}$ |
| MS123 | + | Δ | + | $(0.80\pm0.1)\times10^{-5}$ | $1.0\pm0.09$ | $(0.62\pm0.04)\times10^{-2}$ |
| MS122 | + | + | Δ | $(1.2\pm1.6)\times10^{-5}$ | $0.87\pm0.04$ | $(2.8\pm1.4)\times10^{-4}$ |
| MS135 | Δ | Δ | + | $<(5.6\pm0.31)\times10^{-5}$ | $1.1\pm0.17$ | $0.25\pm0.27$ |
| MS136 | Δ | + | Δ | $<(2.9\pm5.5)\times10^{-5}$ | $0.81\pm0.35$ | $(2.6\pm3.9)\times10^{-2}$ |
| MS124 | + | Δ | Δ | $<(2.5\pm0.10)\times10^{-5}$ | $1.2\pm0.05$ | $(2.0\pm0.02)\times10^{-2}$ |
| MS137 | Δ | Δ | Δ | $<(2.3\pm0.11)\times10^{-5}$ | $1.2\pm0.40$ | $1.1\pm0.63$ |

[a] *E. coli* strains are described in Table 4.
[b] +, wild type; Δ, deletion. Specific alleles used include *polB* (Pol II), Δ*polB*: :Ω; *dinB* (Pol IV), Δ(*dinB-yafN*): :*kan*; and *umuDC* (Pol V), Δ*umuDC595*: :*cat*.
[c] Representative transformants of the indicated strain bearing either the control plasmid (pSU38 [$Kan^R$], pACM [$Cam^R$], or pAMP [$Amp^R$]); the $\beta^+$-(pACYC*dnaN*$^+$ [$Kan^R$], pACM*dnaN*$^+$ [$Cam^R$], or pAMP*dnaN*$^+$ [$Amp^R$]); or the $\beta^{148–152}$-expressing plasmid (pACYCβ5A [$Kan^R$], pACMβ5A [$Cam^R$], or pAMPβ5A [$Amp^R$]) were cultured overnight, and serial dilutions of each were plated onto LB agar containing appropriate antibiotics. Results shown represent the average of duplicates. Values in parentheses represent the range. Cell titers were on the order of $\sim10^9$ cells/ml for all strains except MS134 bearing pACYCβ5A (see footnote d). $Kan^R$ plasmids were used with strains MS120, MS134, MS122, and MS136; $Cam^R$ plasmids were used with strains MS123 and MS135; and $Amp^R$ plasmids were used with strains MS124 and MS137. All plasmids were derived from pSU38, and their salient features are described in Table 4.
[d] Titers of cultures for strain MS134 bearing the $\beta^{148–152}$-expressing plasmid (pACYCβ5A) were on the order of $\sim10^6$ cells/ml, which corresponds to ~1000-fold fewer viable cells than observed for the same strain bearing either the control plasmid (pSU38) at 30 °C or the $\beta^+$-expressing plasmid (pACYC*dnaN*$^+$) at both 30° and 42 °C.

viable at 37 °C due to a *sulA11* mutation.[19] The *dnaN159* strain was moderately impaired for MMS-induced mutagenesis at 30 °C (Fig. 8a), and was severely impaired at 37 °C (Fig. 8b). More importantly, physiological levels of $\beta^+$ expressed from a plasmid restored MMS-induced mutagenesis on the *dnaN159* strain at 37 °C, while expression of $\beta^{148–152}$ did not (Fig. 9a). We next asked whether inactivation of Pol II and/or Pol IV restored MMS-induced mutagenesis in the $\beta^{148–152}$ strain. Similar to UV, inactivation of Pol IV modestly increased the frequency of MMS-induced mutagenesis (Fig. 9b), while inactivation of both Pol II and Pol IV resulted in a robust MMS-induced mutator phenotype in the $\beta^{148–152}$-expressing strain (Fig. 9c). Inactivation of Pol V in this same strain abrogated mutagenesis, confirming that it was Pol V dependent (Fig. 9d). These results, taken together with those discussed above (Fig. 7), support a model in which residues 148-HQDVR-152 of the β clamp play an essential role in coordinating the actions of Pol II, Pol IV, and Pol V with those of Pol III.

## Discussion

Results presented in this report indicate that the ability of the clamp to interact with the DNA template that it encircles is essential for viability of *E. coli* (Fig. 6). In addition, genetic and biochemical characterization of $\beta^{148–152}$ demonstrated that residues H148–R152 also contribute to proper management of the different *E. coli* Pols. Taken together, these findings suggest that clamp–DNA interactions influence the way in which the clamp is positioned on DNA and that this positioning influences the ability of the clamp to manage the actions of the different *E. coli* Pols. Finally, our finding that $\beta^{148–152}$ was impaired for physical interaction with both Pol II and Pol IV (Fig. 4c) suggests that these Pols interact with this surface on the clamp during DNA replication. In the crystal structure of the β clamp in complex with the little finger domain of Pol IV, the α-carboxyl of Pol IV–L351 interacts electrostatically with R152 of the clamp.[38] Our results suggest that this, as well as possibly additional interactions that were not captured in the crystal structure, contribute

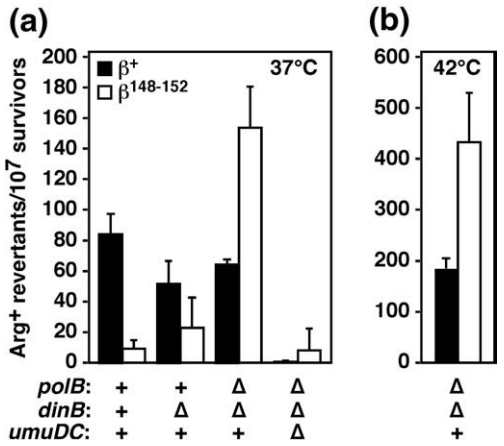


**Fig. 7.** Influence of Pol II, Pol IV, and Pol V on UV-induced mutagenesis in the *danN159* strain expressing $\beta^{148–152}$. UV-induced mutagenesis in isogenic *dnaN159* strains lacking the indicated combinations of the *polB* (Pol II), *dinB* (Pol IV), and *umuDC* (Pol V) alleles and expressing either $\beta^+$ (black bars) or $\beta^{148–152}$ (white bars) are shown. Strains were cultured at either 37 °C (a) or 42 °C (b), and mutagenesis was measured as described in Materials and Methods. Results shown represent the average of duplicates from at least two independent experiments. Error bars represent the standard deviation.

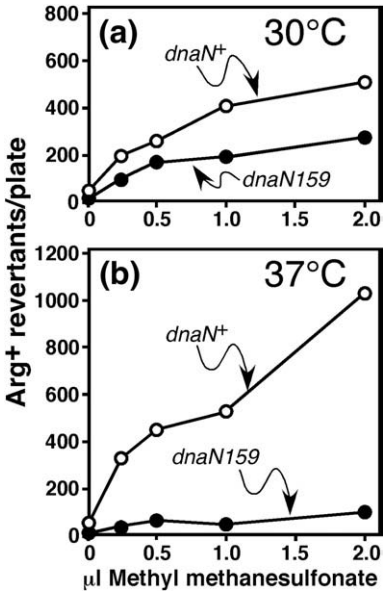


**Fig. 8.** Role of $\beta^+$ and β159 in MMS-induced mutagenesis. Frequencies of MMS-induced mutagenesis in isogenic *dnaN*$^+$ (MS100) and *dnaN159* (MS101) strains cultured at 30 °C (a) or 37 °C (b) were measured as described in Materials and Methods. Representative results are shown.

to Pol IV replication. Alternatively, Pol IV may interact differently with β when it is bound to DNA. Regardless, these findings support a model in which certain partners, such as Pol II and Pol IV, compete with DNA for interaction with residues H148–R152 of the clamp, while others, such as Pol III, do not. Consistent with this model, Georgescu and colleagues[11] previously described how both ssDNA and a synthetic polypeptide corresponding to the C-terminal nine residues of the Pol III α subunit compete for binding to the hydrophobic cleft of β. Thus, taken together, our findings support a model in which a combination of competitive clamp–partner, clamp–DNA, and partner–DNA interactions collectively contribute to the management and coordinate regulation of replicative and TLS Pols.

Although $\beta^{148–152}$ was unable to support viability of *E. coli*, it was nevertheless able to fully complement the temperature-sensitive growth phenotype of the *dnaN159* strain (Table 3), most likely as a β159–$\beta^{148–152}$ heterodimer. Consistent with this conclusion, temperature-resistant growth of the *dnaN159* strain expressing $\beta^{148–152}$ required that Pol II and Pol IV were inactivated (Table 3). Our finding that $\beta^{148–152}$ was unable to stimulate replication by these Pols *in vitro* (Fig. 4) suggests that they impair growth of the $\beta^{148–152}$ strain through contact with β159 in the heterodimer. Consistent with this conclusion, β159 was capable of stimulating replication by Pol II and Pol IV, albeit at reduced levels compared to $\beta^+$.[20] Since the DNA passes through the central hole of the clamp at a pronounced 22° angle,[11] a β159–$\beta^{148–152}$ heterodimer would be capable of contacting both ssDNA, through the cleft of $\beta^{148–152}$, or dsDNA, through residues R24 of β159 or $\beta^{148–152}$, and H148–R152 of β159 (Fig. 1b). Thus, the β159–$\beta^{148–152}$ heterodimer would be largely proficient for interaction with both ssDNA and dsDNA. In contrast, both subunits within the β159 and the $\beta^{148–152}$ homodimers would be largely impaired for either ssDNA or dsDNA binding, respectively. Finally, the β P20L substitution suppresses the temperature-sensitive growth phenotype of the *dnaN159* strain.[20] Given the close proximity of P20 and R24, it seems likely that the P20L substitution in *dnaN783* acts to influence interaction of the mutant clamp with DNA (Fig. 1b), consistent with our model that temperature sensitivity results at least in part due to

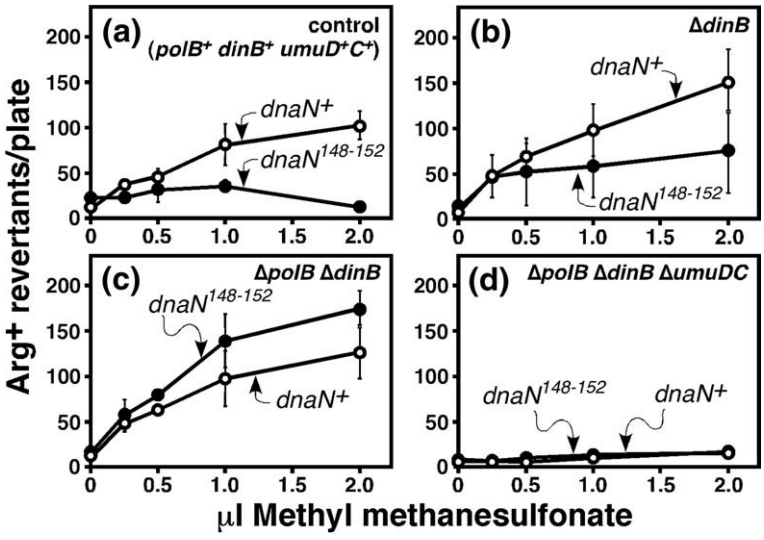


**Fig. 9.** Influence of Pol II, Pol IV, and Pol V on MMS-induced mutagenesis in the $\beta^{148–152}$-expressing strain. The frequency of MMS-induced mutagenesis observed for the *dnaN159* strain expressing $\beta^{148–152}$ (a) or its isogenic derivatives lacking Pol IV (b), Pol II and Pol IV (c), or Pol II, Pol IV, and Pol V (d) are shown. All strains were cultured at 37 °C. Results shown represent the average of duplicates. Error bars represent the range.

impaired β159–DNA interactions, which can be complemented through formation of a β159–$\beta^{148–152}$ heterodimer.

Coordination of Pol III with Pol II, Pol IV, and Pol V was severely impaired in the *dnaN159* strain expressing $\beta^{148–152}$. For example, Pol IV was toxic to the $\beta^{148–152}$-expressing *dnaN159* strain in the absence of Pol II, both at 30 and at 42 °C (Table 3). Furthermore, Pol V-dependent UV- and MMS-induced mutagenesis was essentially eliminated in the *dnaN159* strain expressing $\beta^{148–152}$ (Figs. 7 and 9). However, inactivation of Pol II and Pol IV restored Pol V function (Figs. 7 and 9). Based on SPR experiments, Pol II and Pol IV were impaired for interaction with both β159 and $\beta^{148–152}$ (Table 2).[20] However, β159 was able to support Pol II and Pol IV replication *in vitro*,[20] while $\beta^{148–152}$ was not (Fig. 4). Taken together, these findings suggest that Pol II somehow blocks what amounts to lethal access of Pol IV to the fork and that the combination of Pol II and Pol IV acts to outcompete Pol V for interaction with the β159–$\beta^{148–152}$ clamp. Alternatively, the inability of the β159–$\beta^{148–152}$ clamp to properly coordinate the actions of Pol III with those of Pol II, Pol IV, and Pol V may result from impaired clamp–DNA interactions. These interactions could influence which surfaces of the clamp are exposed and therefore accessible to the different Pols. As a result, a hierarchy could be established, dependent in part on the clamp–DNA complex, in which clamp temporally coordinates access of its different partner proteins to the DNA. An important feature of this model is that DNA structures could differentially influence clamp–partner interactions. In addition, it is likely that these clamp–partner interactions are further complemented by direct interactions between the partner protein and the DNA template. Finally, Georgescu and colleagues suggested that interactions involving R24 and H148–R152 with the DNA could help to promote Pol switching in a toolbelt-like model by 'shuttling' the DNA from one clamp protomer to the other to toggle the DNA primer between Pols that are bound to β.[11] Our results indicate that this type of model is unlikely to function *in vivo*, at least as initially described, due to the fact that Pols and the template DNA compete with each other for common surfaces on the β clamp. Thus, a clear determination of the role(s) of clamp–DNA interactions in Pol switching will require separation-of-function mutations in the clamp that differentially affect DNA and partner protein interactions.

In conclusion, our findings support a model in which a sophisticated combination of competitive clamp–DNA, clamp–partner, and partner–DNA interactions are required for proper management of the different *E. coli* Pols *in vivo*. Our findings also suggest that it is possible to exploit the temperature-sensitive growth phenotype of the *dnaN159* gene product to characterize heterodimeric clamp proteins *in vivo*. This type of approach, coupled with a method for purification of heterodimeric clamp proteins bearing various site-specific mutation(s) in one protomer, and either no mutation or different mutation(s) in the other protomer, would enable detailed dissection of the mechanisms by which the clamp enables Pols to switch places with each other on DNA, as well as other proteins whose actions are coordinated/regulated by the clamp.

## Materials and Methods

### Purification of recombinant proteins

The mutant $\beta^{148–152}$ clamp protein was purified from 4 l of LB supplemented with Amp and inoculated with 80 ml of an overnight culture of BL21(DE3)(pET11a-β5A). The culture was grown at 30 °C with shaking until it reached an $OD_{595}$ ~0.8, at which point IPTG was added to a final concentration of 50 μM. The culture was incubated at 30 °C for an additional 3 h. Cells were harvested by centrifugation, resuspended in TS buffer [25 mM Tris–HCl (pH 8.0), 20% sucrose], and lysed by double passage through a chilled French press. After centrifugation at 15,000 rpm for 30 min at 4 °C, the soluble fraction was adjusted to 70% ammonium sulfate. Precipitated $\beta^{148–152}$ recovered by centrifugation was resuspended in buffer A [10 mM sodium phosphate (pH 6.8), 1 mM ethylenediaminetetraacetic acid (EDTA), 1 mM DTT], and dialyzed against the same buffer containing 25 mM NaCl overnight at 4 °C. After centrifugation, $\beta^{148–152}$ was applied to a 20-ml HiTrap Capto-Q column (GE Healthcare) equilibrated in buffer A containing 25 mM NaCl. The column was washed with 10 column volumes of the same buffer, and $\beta^{148–152}$ bound to the column was eluted stepwise with buffer A containing 0.5 M NaCl. Fractions containing $\beta^{148–152}$ were identified by SDS-PAGE, pooled, dialyzed against buffer A containing 25 mM NaCl, and loaded onto an HR 16/10 MonoQ column (GE Healthcare) equilibrated in the same buffer. $\beta^{148–152}$ was eluted with buffer A using a linear gradient of 25 to 500 mM NaCl. Fractions containing $\beta^{148–152}$ were identified by SDS-PAGE, pooled, dialyzed against buffer A containing 25 mM NaCl, and applied to a 5-ml HiTrap Heparin column (GE Healthcare). $\beta^{148–152}$ present in the flow-through was precipitated with 70% ammonium sulfate, resuspended in buffer A, and applied to an HR 10/30 Superose 12 column (GE Healthcare) equilibrated in buffer A containing 100 mM NaCl. Fractions containing $\beta^{148–152}$ were identified by SDS-PAGE, pooled, and dialyzed against buffer B [20 mM Tris–HCl (pH 7.5), 0.5 mM EDTA, 0.5 mM DTT, 20% glycerol]. The concentration of $\beta^{148–152}$ (4 mg/ml) was determined by Bradford assay and densitometric analysis of Coomassie Blue R-250-stained SDS-PAGE relative to a standard curve made using bovine serum albumin (BSA) (Pierce).

SPR clamp loading experiments used untagged forms of the clamp, purified as described above for $\beta^{148–152}$. N-terminal $His_6$ and cAMP-dependent kinase motif tagged forms of $\beta^{+}$ and $\beta^{148–152}$ were expressed from $p\beta^{HMK}$ and $p\beta5A^{HMK}$, respectively. These forms of the clamp were used for the SPR clamp–partner protein interaction experiments and were purified from 2 l of culture using the same protocol described above, with the addition of an initial affinity chromatography step using a 1-ml HiTrap cobalt column (GE Healthcare) as described previously.[20] The $\tau_2\gamma\delta\delta'\chi\psi$,[20,39] $\gamma_3\delta\delta'\chi\psi$, and $\gamma_3\delta\delta'$ forms of the DnaX clamp loader complex,[20] Pol III* [$\tau_2\gamma\delta\delta'\chi\psi(\alpha\varepsilon\theta)_2$],[39] Pol III core ($\alpha\varepsilon\theta$),[20] Pol II,[20] and Pol IV[20] were overproduced and purified as described in the indicated reference.

ssDNA binding protein was overproduced using *E. coli* strain BL21(DE3) (Novagen) bearing plasmid pEAW134 provided by Dr. Michael Cox (University of Wisconsin, Madison, WI) and was purified as described.[40]

### Structural determination of the mutant $\beta^{148–152}$ clamp protein

$\beta^{148–152}$ was crystallized in hanging-drop vapor-diffusion experiments using conditions reported for the wild-type β clamp protein.[12] The best crystals were obtained from hanging-drop vapor diffusion of 2 μl protein solution at 4 mg/ml with 2 μl buffer B. The reservoir solution was 13% isopropanol, 100 mM $CaCl_2$, 100 mM Mes (pH 6.5). The crystals were cryoprotected with 16–24% MPD (methyl-2,4-pentanediol) before flash-freezing. Frozen crystals were screened using the Stanford Automated Mounter[41] operated by Blu-Ice.[42] Data to 1.76 Å resolution were collected on a single crystal at the Stanford Synchrotron Radiation Laboratory (SSRL), beamline 9.2. Diffraction images were collected with a 1.0° oscillation range using a Mar325 CCD detector, with an exposure time of 10 s and a crystal-to-detector distance of 200 mm, with a wavelength of 1.00 Å. Data were indexed and scaled with HKL-2000.[43] Full details regarding the structure are given in Table 1; no cutoff was applied and the Wilson *B*-factor is estimated as 35.0 $Å^2$. The structure was solved by molecular replacement using Molrep[44] as implemented in CCP4[45] using the wild-type homodimeric protein as the search model [Protein Data Bank (PDB) code 1ok7].[21] The structure was refined with REFMAC5[46,47] and manually rebuilt with Coot.[48] The number of residues observed for chains A and B was 366, respectively. In addition, the structure contains 381 modeled water molecules and two sets of $CaCl_2$ atoms. Structural figures were produced using PyMOL (DeLano).

### SPR analysis of β clamp–partner interactions

All SPR binding assays were carried out at 25°C on a BIAcore X biosensor instrument (GE Healthcare) using HBS-EP [10 mM Hepes (pH 7.4), 150 mM NaCl, 3 mM EDTA, 0.005% (v/v) surfactant P20] as running buffer. Approximately 5000 RU of BSA-free anti-Penta-His antibody (Qiagen) was covalently immobilized in both flow cells (Fc1 and Fc2) to a CM5 sensor chip surface (GE Healthcare) by amine coupling according to the manufacturer's recommendations. The antibody surface in one flow cell (Fc2) was used to capture the $His_6$-tagged β clamps at a flow rate of 5 μl/min, while the antibody in the other flow cell (Fc1) was left blank for background subtraction. Immediately following capture, the indicated concentrations of the noted clamp partner protein were injected over both flow cells for 120 s at a flow rate of 30 μl/min. Following each interaction cycle, the antibody surface was regenerated by injection of 10 mM glycine–HCl (pH 1.5) for 1 min at a flow rate of 50 μl/min to remove all clamps and interacting proteins. Fresh β dimer was captured for each separate interaction experiment. This method allows the clamp to be immobilized in a homogenous orientation and ensured that the dimeric form of the clamp was present, thus permitting kinetic analysis.

Various concentrations of Pol II (1 nM to 2.5 μM) or Pol IV (15 nM to 1.5 μM) were injected over ~250 and ~500 RU, respectively, of antibody-captured $\beta^+$ or $\beta^{148–152}$ clamp. Kinetic values were obtained by fitting the SPR curves to the 1:1 Langmuir binding model using the BIAevaluation software (version 4.1). The $R_{max}$ was changed from a global to a local parameter in all curve fits to account for slight variations in the amount of β captured on the chip surface in each experiment.

Kinetic values for wild-type β– and $\beta^{148–152}$–DnaX interactions were obtained from injections of 1–400 nM clamp loader complex ($\gamma_3\delta\delta'\chi\psi$) over ~100 RU of β clamp. For these experiments, the HBS-EP running buffer lacked EDTA and was supplemented with 10 mM $MgCl_2$ and 1 mM ATP. Equilibrium dissociation constants were obtained using the steady-state model because rates were too rapid to fit the curves using the simultaneous $k_a$ and $k_d$ 1:1 binding model. The off rates were determined by separately fitting the dissociation part of the binding curves, and on rates were then calculated using the equation $K_D = k_d/k_a$.

### SPR clamp loading assay

DNA oligonucleotides used for clamp loading were synthesized by Sigma and were gel-purified. The primed DNA template was constructed by combining 250 nM of the 3′-biotinylated 80-mer (Table 4) with a 10-fold molar excess of the complimentary 30-mer (Table 4) for 5 min at 95 °C in 100 mM NaCl. The DNA substrate was diluted to 5 nM in HBS-EP and ~500 RU was immobilized at a flow rate of 10 μl/min in Fc2 on the streptavidin surface of a Sensor Chip SA (GE Healthcare). The DnaX clamp loader complex (50 nM of $\gamma_3\delta\delta'\chi\psi$) was preincubated for 5 min on ice with β (250 nM of $\beta^+$, β159, or $\beta^{148–152}$, as indicated) in HBS-EP lacking EDTA and supplemented with 1 mM ATP and 10 mM $MgCl_2$. Premixes were injected for 2 min at a flow rate of 10 μl/min to monitor association of DnaX–β complex with DNA, as well as loading and dissociation of β on DNA. A regeneration step to remove β was not necessary because the clamp slid off the free nonbiotinylated 5′ end of the 80-mer DNA template strand during buffer wash.

### *In vitro* primer extension assay

The ability of $\beta^+$ or $\beta^{148–152}$ to stimulate replication by Pol III, Pol II, or Pol IV was measured as described previously. Briefly, reactions (20 μl) containing replication assay buffer [20 mM Tris–HCl (pH 7.5), 8.0 mM $MgCl_2$, 0.1 mM EDTA, 5 mM DTT, 1 mM ATP, 5% glycerol, and 0.8 μg/ml BSA] were supplemented with 0.133 mM [$^3$H] dTTP–deoxynucleotide triphosphates (111.7 CPM/pmol), 2 μM ssDNA binding protein, and 5 nM of SP20-primed M13 ssDNA. M13 ssDNA was purified from intact phage by extraction with phenol–chloroform, precipitation in ethanol, and gel filtration with Superose-12 (GE Healthcare). Reactions were initiated by addition of the indicated Pol. When noted, 5 min was provided for clamp loading prior to addition of the indicated Pol. Reaction products were spotted onto DE81 (VWR) paper, washed four times in 0.5 M dibasic sodium phosphate, and quantitated by liquid scintillation spectroscopy.[26]

### Bacterial strains

*E. coli* strains used in this study, described in Table 4, were routinely grown in LB medium.[49] When necessary, the following antibiotics were used at the indicated concentrations: ampicillin (Amp), 150 μg/ml; chloramphenicol (Cam), 10 or 20 μg/ml (as indicated); kanamycin

**Table 4.** *E. coli* strains and plasmid DNAs used in this study

*E. coli* strains

| Strain | Relevant genotype | Source or construction |
|---|---|---|
| BL21(DE3) | $F^-$ *ompT hsdS*$_B$($r_B^-$ m$_B^-$) *gal dcm* (DE3) | Novagen |
| MS100 | *xyl-5 mtl-1 galK2 rpsL31* Δ(*gpt-proA*)*62 lacY1 tsx-33 supE44 thi-1 hisG4*(Oc) *argE3*(Oc) *araD139 thr-1 sulA211 dnaN*$^+$ *tnaA300*::Tn*10* | 28 |
| MS101 | MS100: *dnaN159 tnaA300*::Tn*10* | 28 |
| AB1157 | *xyl-5 mtl-1 galK2 rpsL31 kdgK51 lacY1 tsx-33 supE44 thi-1 leuB6 hisG4*(Oc) *mgl-51 argE3*(Oc) *rfbD1 proA2 ara-14 thr-1 qsr-9 qin-111* | CGSC[31] |
| MS119 | AB1157: *dnaN*$^+$ *tnaA300*::Tn*10* | 19 |
| MS120 | AB1157: *dnaN159 tnaA300*::Tn*10* | 19 |
| MS134 | AB1157: *dnaN159 tnaA300*::Tn*10* Δ*polB*::Ω | This work |
| MS123 | AB1157: *dnaN159 tnaA300*::Tn*10* Δ(*dinB-yafN*)::*kan* | 19 |
| MS122 | AB1157: *dnaN159 tnaA300*::Tn*10* Δ*umuDC595*::*cat* | 19 |
| MS135 | AB1157: *dnaN159 tnaA300*::Tn*10* Δ*polB*::Ω Δ(*dinB-yafN*)::*kan* | This work |
| MS136 | AB1157: *dnaN159 tnaA300*::Tn*10* Δ*polB*::Ω Δ*umuDC595*::*cat* | This work |
| MS124 | AB1157: *dnaN159 tnaA300*::Tn*10* Δ(*dinB-yafN*)::*kan* Δ*umuDC595*::*cat* | 19 |
| MS137 | AB1157: *dnaN159 tnaA300*::Tn*10* Δ*polB*::Ω Δ(*dinB-yafN*)::*kan* Δ*umuDC595*::*cat* | This work |
| MS138 | AB1157: *dnaN*$^+$*-tet-recF*$^+$ | This work |
| MS139 | AB1157: *lamB*::(His$_6$-*dnaN*$^+$-*cat*) | This work |
| MS140 | AB1157: Δ*polB*::Ω Δ(*dinB-yafN*)::*kan* | This work |
| MS141 | AB1157: Δ*polB*::Ω Δ(*dinB-yafN*)::*kan lamB*::(His$_6$-*dnaN*$^+$-*cat*) | This work |
| MS142 | AB1157: Δ*polB*::Ω Δ(*dinB-yafN*)::*kan lamB*::(His$_6$-*dnaN*$^+$-*cat*) *dnaN*$^+$*-tet-recF*$^+$ | This work |
| MS143 | AB1157: Δ*polB*::Ω Δ(*dinB-yafN*)::*kan lamB*::(His$_6$-*dnaN*$^+$-*cat*) *dnaN*$^{148–152}$*-tet-recF*$^+$ | This work |
| MS144 | AB1157: Δ*polB*::Ω Δ(*dinB-yafN*)::*kan dnaN*$^+$*-tet-recF*$^+$ (pJD100) | This work |
| MS145 | AB1157: Δ*polB*::Ω Δ(*dinB-yafN*)::*kan dnaN*$^{148-152}$*-tet-recF*$^+$ (pJD100) | This work |

Plasmid DNAs

| Plasmid | Relevant features | Source or construction |
|---|---|---|
| pET11a | Amp$^R$, ColE1 origin, directs overexpression of cloned gene under control of a T7 promoter | Novagen |
| pET11a-β5A | Amp$^R$, pET11a derivative overexpressing $\beta^{148–152}$ from the T7 promoter | This work |
| $p\beta^{HMK}$ | Amp$^R$, pET16b derivative overexpressing $\beta^+$ with an N-terminal His$_6$ and kinase tag | 32 |
| $p\beta5A^{HMK}$ | Amp$^R$, $p\beta^{HMK}$ derivative overexpressing $\beta^{148–152}$ | This work |
| pSU38 | Kan$^R$, p15A origin, cloning vector | 33 |
| pACYC*dnaN*$^+$ | Kan$^R$, pSU38 derivative expressing physiological levels of $\beta^+$ | 19 |
| pACMβ5A | Kan$^R$, pSU38 derivative expressing physiological levels of $\beta^{148–152}$ | 19 |
| pACM | Cam$^R$, pSU38 derivative containing the *cat* gene inserted in *kan* | 19 |
| pACM*dnaN*$^+$ | Cam$^R$, pACM derivative expressing physiological levels of $\beta^+$ | 19 |
| pACMβ5A | Cam$^R$, pACM derivative expressing physiological levels of $\beta^{148–152}$ | 19 |
| pAMP | Amp$^R$, pSU38 derivative containing the *bla* gene inserted in *kan* | 19 |
| pAMP*dnaN*$^+$ | Amp$^R$, pAMP derivative expressing physiological levels of $\beta^+$ | 19 |
| pAMPβ5A | Amp$^R$, pAMP derivative expressing physiological levels of $\beta^{148–152}$ | 19 |
| pRD46 | Amp$^R$, pSC101 origin, *repA*(Ts), expresses λ Red recombinase function under control of *araBADC* promoter | 27 |
| pAB1 | Tet$^R$, pBR322 derivative containing 7.8-kb *PstI dnaA71*(Cs, Sx) *dnaN*$^+$ *recF*$^+$ *gyrB*$^+$ cassette | 34 |
| pANTF | Kan$^R$ Tet$^R$, pACYC*dnaN*$^+$ derivative containing *dnaA*$^+$*-dnaN*$^+$*-tet-recF*$^+$ cassette | This work |
| pANβ5TF | Kan$^R$ Tet$^R$, pANTF derivative containing *dnaA*$^+$*-dnaN*$^{148–152}$*-tet-recF*$^+$ cassette | This work |
| pANβ5PVUIITF | Kan$^R$ Tet$^R$, pANβ5TF derivative containing a copy of the *dnaA*$^+$*-dnaN*$^{148–152}$*-tet-recF*$^+$ cassette with a silent mutation within *dnaN*$^{148–152}$ that disrupts a PvuII restriction site | This work |
| pRMB100-Cat | Kan$^R$ Cam$^R$, pSU38 derivative containing *lamB*::(His$_6$-*dnaN*$^+$-*cat*) cassette | This work |
| pWSK29 | Amp$^R$, pSC101 origin, low-copy-number cloning vector | 35 |
| pJD100 | Amp$^R$, pSC101 origin, expresses physiological levels of *dnaN*$^+$ | 28 |
| pKOV | CamR, pSC101 origin, *repA*(Ts) | 36 |

Oligonucleotides

| Primer | Nucleotide sequence |
|---|---|
| 80-mer | 5′-[T$_{30}$]CTCCCTTCTTCTCCTCCCTCTCCCTTCCC[T$_{21}$]-biotin-3′ |
| 30-mer | 5′-AGGGAAGGGAGAGGGAGGAGAAGAAGGGAG-3′ |
| SP20 | 5′-ACGCCTGTAGCATTCCACAG-3′ |
| D150 loop top | 5′-CTATGGCGGCTGCGGCCGCTGCCTATTACTAAATGG-3′ |
| D150 loop bottom | 5′-CCATTTAAGTAATAGGCAGCGGCCGCAGCCGCCATAG-3′ |
| Tet top | 5′-GCACCTCGAGTCAGCCCCATA-3′ |
| Tet bottom | 5′-GAGTGGTGAATTCGTTAGCG-3′ |
| RecF top | 5′-GAGCGCGAATTCTGTTGTCATGCC-3′ |
| RecF bottom | 5′-CAACGTTTCTCGAGCATTTATACTTGG-3′ |
| D150ΔPvuII top | 5′-CGTGCAACTAGAAGGTGAACGGATGCTGGTACGCTCCGG-3′ |
| D150ΔPvuII bottom | 5′-CCGGAGCGTACCAGCATCCGTTCACCTTCTAGTTGCACG-3′ |
| JK28+2 | 5′-CATTGCCAATGCCAACTTTACC-3′ |
| RecF back | 5′-CTTCGAATTTTCGTCCGACATGTC-3′ |

*(continued on next page)*

**Table 4** (*continued*)

| Primer | Nucleotide sequence |
|---|---|
| DnaAP | 5′-CATGAATGTTTCAGCCTTAGTC-3′ |
| LamB-1 | 5′-CTCGCGCAAACTTCCTCTGGCGGTTGCCG-3′ |
| LamB-2 | 5′-GAGACAAAGCTTGAGACGCGTGAGGTCGACGAGGGGTTGA TTTCCATCTGCGCTAAACGCACATCG-3′ |
| LamB-7 | 5′-GAGACAACGCGTGAGGGATCCACACGTGCCAACTTGCGTG ATAACTATCGTCTGG-3′ |
| LamB-8 | 5′-AGTGCCAAGCTTGAGCCATCTGGGCACCGAAGGTCCACTC GTC-3′ |
| Cat promoter | 5′-GAATTCGGATCCGTCTGCTATGTGGTGCTAT-3′ |
| Cat end | 5′-GAATTCGGATCCCTTATTCAGGCGTAGCACCAGGCG-3′ |
| LamB-DN | 5′-GAATGCGGCGTAAACGCCTTATCC-3′ |

CGSC, *E. coli* Genetic Stock Center, Yale University, New Haven, CT, USA.

(Kan), 40 μg/ml; tetracycline (Tet), 2.5 μg/ml; and spectinomycin (Spec), 20 μg/ml. When noted, strains were grown in M9 minimal salt medium supplemented with 0.2% maltose or glucose, as noted, 5 μg/ml thiamine, and 40 mg/ml of each of the following amino acids: arginine, histidine, isoleucine, leucine, proline, threonine, and valine.[49] Generalized transduction using P1*vir* was performed as described previously.[49]

### Construction of plasmids

Plasmid cloning was achieved using standard molecular biology techniques.[50] The salient features of each plasmid as well as the sequence of synthetic oligonucleotide primers used for cloning or diagnostic PCR are indicated in Table 4. The sequence of each PCR product used for cloning was verified by automated nucleotide sequence analysis (Roswell Park Biopolymer Facility). Plasmid $p\beta5A^{HMK}$ expresses an N-terminally $His_6$ and cAMP-dependent kinase tagged form of $\beta^{148–152}$ from a T7 RNA polymerase promoter. It was cloned using the QuickChange technique (Stratagene). PCR reactions contained primers D150 loop top and D150 loop bottom (Table 4), and plasmid $p\beta^{HMK}$ served as template. Plasmid pET11a-β5A expresses an untagged form of $\beta^{148–152}$ from a T7 RNA polymerase promoter. It was constructed by subcloning an NdeI-BamHI fragment containing $dnaN^{148–152}$ from $p\beta5A^{HMK}$ into pET11a.

Plasmid pANTF contains a *′dnaA-dnaN-tet-recF* cassette. The sequence upstream of *recF* bearing the Shine–Dalgarno sequence is duplicated, and one copy is located upstream of *tet* (lower case text), while the second copy is upstream of *recF* (upper case text; Fig. 5a). pANTF was constructed by inserting a *tet-recF* cassette into the unique SalI site located at the 3′ end of the *dnaN* allele in pACYC$dnaN^+$. The *tet* gene was PCR-amplified from pACYC184 (nucleotide positions 1421–2789) using primers Tet top and Tet bottom, while *recF* was PCR-amplified from plasmid pAB1 using primers RecF top and RecF bottom. Primers Tet bottom and RecF Top each contain an internal EcoRI site. The *tet* and *recF* PCR fragments were digested with EcoRI and ligated together *in vitro* using T4 DNA ligase, and the ligation product was used as template for PCR with primers Tet top and RecF bottom. The *tet-recF* cassette was digested with SalI, which cuts upstream of *tet* (within Tet top), and XhoI, which cuts downstream of *recF* (within RecF bottom), prior to its ligation into the SalI site of pACYC$dnaN^+$. The orientation of the *tet* cassette was determined by restriction mapping. Plasmid pANβ5ATF is a pANTF derivative that contains the *′dnaA-*$dnaN^{148–152}$*-tet-recF* cassette. It was cloned by the QuickChange procedure (Stratagene) using primers D150 loop top and D150 loop bottom. Plasmid pANβ5APVUIITF is a pANβ5ATF derivative that contains two silent base substitution mutations that disrupt a PvuII restriction site (CAGCTG→CA*A*CT*A*) overlapping amino acid positions 91–92 located ~170 nucleotides upstream of the 148-HQDVR-152 poly-Ala substitutions (Fig. 5a). This polymorphism was used as a diagnostic marker to monitor for the presence of the $dnaN^{148–152}$ mutation on the chromosome (Fig. 5b). It was cloned using the QuickChange procedure (Stratagene) and primers D150ΔPvuII top and D150ΔPvuII bottom.

Plasmid pRMB100-Cat encodes the *lamB*: :($His_6$-$dnaN^+$-*cat*) allele. It was constructed as follows: the upstream region of *lamB*, corresponding to the first 623 nucleotides of the *lamB* coding sequence, was PCR-amplified from genomic DNA isolated from *E. coli* strain MG1655 (obtained from the *E. coli* Genetic Stock Center) using primers LamB-1 and LamB-2. The downstream region of *lamB* corresponding to nucleotides 658 through the stop codon at position 1341 was similarly amplified using primers LamB-7 and LamB-8. The *cat* allele (nucleotide positions 5487–935) was PCR-amplified from pKOV[36] using primers Cat promoter and Cat end, which introduce a BamHI site at each end of the cassette. PCR fragments were initially cloned into pCR-Blunt II-TOPO (Invitrogen). They were subsequently subcloned into pSU38 stepwise as follows: the upstream portion of *lamB* was inserted into the EcoRI-SalI sites, followed by a SalI-BamHI $His_6$-*dnaN* fragment initially derived from $p\beta^{HMK}$, the BamHI-HindIII downstream *lamB* fragment, and finally, the BamHI *cat* fragment, which was inserted in between the $His_6$-*dnaN* and downstream *lamB* fragments. Restriction digestion analysis confirmed that the *cat* allele was inserted in the same orientation as *lamB* and *dnaN*.

### Phage λ Red-mediated construction of *E. coli* strains

Phage λ Red-mediated recombination was performed as described by Datsenko and Wanner using plasmid pRD46.[27] The initial construction of strains bearing the $dnaN^+$-*tet-*$recF^+$ allele was performed as follows: the 3942-bp *dnaA-*$dnaN^+$*-tet-recF* cassette was PCR-amplified from pANTF using primers JK28+2 and RecF back (Fig. 5a). The gel-purified fragment was then electroporated into strain AB1157 bearing plasmid pRD46, which expresses λ Red function under control of the *araBADC* promoter, using a BioRad gene pulser (2.5 kV, 25 μF, 200 Ω) equipped with 0.2-cm cuvettes (BioRad), as described previously. Recombinants resulting from double crossover were selected on LB plates containing 2.5 μg/ml Tet at 30 °C. The correct structure of the recombinant allele was confirmed by diagnostic PCR using primers DnaAP and RecF bottom,

followed by PvuII digestion (Fig. 5a) and automated nucleotide sequence analysis (Roswell Park Biopolymer Facility). The *dnaN*$^{+}$*-tet* allele was transferred between *E. coli* strains via generalized transduction using P1*vir* by selecting for Tet$^{R}$.

For construction of strains bearing the *lamB*: :(His$_6$-*dnaN*$^{+}$*-cat*) allele, the 4068-bp *lamB*-His$_6$-*dnaN*$^{+}$*-cat-lamB* cassette was PCR-amplified from pRMB100-Cat using primers LamB-1 and LamB-8 (Fig. 5c). It was then electroporated in strain AB1157(pRD46) as described above. Recombinants resulting from double crossover were selected on LB plates containing 10 μg/ml Cam at 37 °C. The correct structure of the recombinant allele *lamB*: :(His$_6$-*dnaN*$^{+}$*-cat*) was confirmed by diagnostic PCR using primers Cat promoter and LamB-DN (Fig. 5c). The *lamB*: :(His$_6$-*dnaN*$^{+}$*-cat*) allele was transferred between strains via generalized transduction using P1*vir* by selecting for Cam$^{R}$. The 3942-bp *dnaA-dnaN*$^{148–152}$*-tet-recF* cassette was PCR-amplified from pANβ5PVUIITF using primers JK28+2 and RecF Back and electroporated into strain MS138(pRD46), which bears *lamB*: :(His$_6$-*dnaN*$^{+}$*-cat*), exactly as described above, except that recombinant strains were selected on M9 minimal plates supplemented with the required amino acids, maltose, and 10 μg/ml Cam, and 2.5 μg/ml Tet at 30 °C. Recombinant strains were screened by diagnostic PCR, PvuII restriction, and automated nucleotide sequence analysis as described above. Plasmid pRD46 was cured from each strain by plating the recombinant strain at 42 °C in the absence of ampicillin, as described,[27] and the *dnaN*$^{148–152}$*-tet* allele was transferred between *E. coli* strains via generalized transduction using P1*vir* by selecting for Tet$^{R}$.

### UV- and MMS-induced mutagenesis

UV-induced mutation frequencies were determined as described previously.[19] MMS-induced mutation frequencies were measured by mixing 100-μl aliquots of overnight cultures with 2.5 ml F top agar (0.8 g/ml NaCl, 0.7% Difco agar) containing 40 μg/ml each of histidine, isoleucine, leucine, proline, threonine, and valine, 2.5 μg/ml arginine, 40 μg/ml thiamine, and the indicated concentration of MMS (Sigma-Aldrich) prior to overlaying onto M9 minimal plates and incubating overnight at the indicated temperature.[37]

## Acknowledgements

This work was supported by NIH grants RO1GM066094, R56GM066094 (M.D.S.), and F31GM073586 (S.K.S.P.) and Interdisciplinary Research Development Fund Grant UB2020 #35905 from the Office of the Vice President for Research at the University at Buffalo, SUNY (M.D.S. and V.C.). We thank the members of our laboratories for helpful discussions, Robert Maul (University at Buffalo, SUNY) for cloning plasmid pET11a-β5A, Barry Wanner (Purdue University) for plasmid pRD46, Andrew Wright (Tufts University) and Steven Sandler (University of Massachusetts, Amherst) for advice regarding strain construction using the λ Red recombination system, Michael Cox (University of Wisconsin, Madison) for plasmid pEAW134, and Ana Gonzalez for help at the SSRL beamline during data collection. SSRL is a national user facility operated by Stanford University on behalf of the U.S. Department of Energy, Office of Basic Energy Sciences, and by the NIH, National Center for Research Resources, Biomedical Technology Program, and by the National Institute of General Medical Sciences.

## References

1. McHenry, C. S. (2003). Chromosomal replicases as asymmetric dimers: studies of subunit arrangement and functional consequences. *Mol. Microbiol.* **49**, 1157–1165.
2. Friedberg, E. C., Walker, G. C., Siede, W., Wood, R. D., Schultz, R. A. & Ellenberger, T. (2006). *DNA Repair and Mutagenesis.* ASM Press, Washington, DC.
3. Sutton, M. D., Smith, B. T., Godoy, V. G. & Walker, G. C. (2000). The SOS response: recent insights into umuDC-dependent mutagenesis and DNA damage tolerance. *Annu. Rev. Genet.* **34**, 479–497.
4. Sutton, M. D. & Walker, G. C. (2001). Managing DNA polymerases: coordinating DNA replication, DNA repair, and DNA recombination. *Proc. Natl Acad. Sci. USA*, **98**, 8342–8349.
5. Friedberg, E. C., Wagner, R. & Radman, M. (2002). Specialized DNA polymerases, cellular survival, and the genesis of mutations. *Science*, **296**, 1627–1630.
6. Dalrymple, B. P., Kongsuwan, K., Wijffels, G., Dixon, N. E. & Jennings, P. A. (2001). A universal protein–protein interaction motif in the eubacterial DNA replication and repair systems. *Proc. Natl Acad. Sci. USA*, **98**, 11627–11632.
7. Wagner, J., Fujii, S., Gruz, P., Nohmi, T. & Fuchs, R. P. (2000). The beta clamp targets DNA polymerase IV to DNA and strongly increases its processivity. *EMBO Rep.* **1**, 484–488.
8. Becherel, O. J., Fuchs, R. P. & Wagner, J. (2002). Pivotal role of the beta-clamp in translesion DNA synthesis and mutagenesis in *E. coli* cells. *DNA Repair (Amst.)*, **1**, 703–708.
9. Lopez de Saro, F. J., Georgescu, R. E., Goodman, M. F. & O'Donnell, M. (2003). Competitive processivity-clamp usage by DNA polymerases during DNA replication and repair. *EMBO J.* **22**, 6408–6418.
10. Lopez de Saro, F. J., Marinus, M. G., Modrich, P. & O'Donnell, M. (2006). The beta sliding clamp binds to multiple sites within MutL and MutS. *J. Biol. Chem.* **281**, 14340–14349.
11. Georgescu, R. E., Kim, S. S., Yurieva, O., Kuriyan, J., Kong, X. P. & O'Donnell, M. (2008). Structure of a sliding clamp on DNA. *Cell*, **132**, 43–54.
12. Kong, X. P., Onrust, R., O'Donnell, M. & Kuriyan, J. (1992). Three-dimensional structure of the beta subunit of *E. coli* DNA polymerase III holoenzyme: a sliding DNA clamp. *Cell*, **69**, 425–437.
13. O'Donnell, M. & Kuriyan, J. (2006). Clamp loaders and replication initiation. *Curr. Opin. Struct. Biol.* **16**, 35–41.
14. Pritchard, A. E. & McHenry, C. S. (2001). Assembly of DNA polymerase III holoenzyme: co-assembly of gamma and tau is inhibited by DnaX complex accessory proteins but stimulated by DNA polymerase III core. *J. Biol. Chem.* **276**, 35217–35222.
15. Kazmirski, S. L., Zhao, Y., Bowman, G. D., O'Donnell, M. & Kuriyan, J. (2005). Out-of-plane motions in open

sliding clamps: molecular dynamics simulations of eukaryotic and archaeal proliferating cell nuclear antigen. *Proc. Natl Acad. Sci. USA*, **102**, 13801–13806.
16. Bowman, G. D., O'Donnell, M. & Kuriyan, J. (2004). Structural analysis of a eukaryotic sliding DNA clamp–clamp loader complex. *Nature*, **429**, 724–730.
17. Bowman, G. D., Goedken, E. R., Kazmirski, S. L., O'Donnell, M. & Kuriyan, J. (2005). DNA polymerase clamp loaders and DNA recognition. *FEBS Lett.* **579**, 863–867.
18. Fujii, S. & Fuchs, R. P. (2004). Defining the position of the switches between replicative and bypass DNA polymerases. *EMBO J.* **23**, 4342–4352.
19. Sutton, M. D., Duzen, J. M. & Maul, R. W. (2005). Mutant forms of the *Escherichia coli* beta sliding clamp that distinguish between its roles in replication and DNA polymerase V-dependent translesion DNA synthesis. *Mol. Microbiol.* **55**, 1751–1766.
20. Maul, R. W., Ponticelli, S. K., Duzen, J. M. & Sutton, M. D. (2007). Differential binding of *Escherichia coli* DNA polymerases to the beta-sliding clamp. *Mol. Microbiol.* **65**, 811–827.
21. Burnouf, D. Y., Olieric, V., Wagner, J., Fujii, S., Reinbolt, J., Fuchs, R. P. & Dumas, P. (2004). Structural and biochemical analysis of sliding clamp/ligand interactions suggest a competition between replicative and translesion DNA polymerases. *J. Mol. Biol.* **335**, 1187–1197.
22. Oakley, A. J., Prosselkov, P., Wijffels, G., Beck, J. L., Wilce, M. C. & Dixon, N. E. (2003). Flexibility revealed by the 1.85 Å crystal structure of the beta sliding-clamp subunit of *Escherichia coli* DNA polymerase III. *Acta Crystallogr., Sect. D: Biol. Crystallogr.* **59**, 1192–1199.
23. Forger, J. M., III, Choie, D. D. & Friedberg, E. C. (1976). Non-histone chromosomal proteins of chemically transformed neoplastic cells in tissue culture. *Cancer Res.* **36**, 258–262.
24. Jeruzalmi, D., Yurieva, O., Zhao, Y., Young, M., Stewart, J., Hingorani, M. *et al.* (2001). Mechanism of processivity clamp opening by the delta subunit wrench of the clamp loader complex of *E. coli* DNA polymerase III. *Cell*, **106**, 417–428.
25. Gomes, X. V. & Burgers, P. M. (2001). ATP utilization by yeast replication factor C: ATP-mediated interaction with DNA and with proliferating cell nuclear antigen. *J. Biol. Chem.* **276**, 34768–34775.
26. Nelson, S. W., Kumar, R. & Benkovic, S. J. (2008). RNA primer handoff in bacteriophage T4 DNA replication: the role of single-stranded DNA-binding protein and polymerase accessory proteins. *J. Biol. Chem.* **283**, 22838–22846.
27. Datsenko, K. A. & Wanner, B. L. (2000). One-step inactivation of chromosomal genes in *Escherichia coli* K-12 using PCR products. *Proc. Natl Acad. Sci. USA*, **97**, 6640–6645.
28. Sutton, M. D. (2004). The *Escherichia coli dnaN159* mutant displays altered DNA polymerase usage and chronic SOS induction. *J. Bacteriol.* **186**, 6738–6748.
29. Maul, R. W. & Sutton, M. D. (2005). Roles of the *Escherichia coli* RecA protein and the global SOS response in effecting DNA polymerase selection in vivo. *J. Bacteriol.* **187**, 7607–7618.
30. Sutton, M. D. & Duzen, J. M. (2006). Specific amino acid residues in the beta sliding clamp establish a DNA polymerase usage hierarchy in *Escherichia coli*. *DNA Repair (Amst.)*, **5**, 312–323.
31. Bachmann, B. J. (1990). Linkage map of *Escherichia coli* K-12, edition 8. *Microbiol. Rev.* **54**, 130–197.
32. Turner, J., Hingorani, M. M., Kelman, Z. & O'Donnell, M. (1999). The internal workings of a DNA polymerase clamp-loading machine. *EMBO J.* **18**, 771–783.
33. Bartolome, B., Jubete, Y., Martinez, E. & de la Cruz, F. (1991). Construction and properties of a family of pACYC184-derived cloning vectors compatible with pBR322 and its derivatives. *Gene*, **102**, 75–78.
34. Gines-Candelaria, E., Blinkova, A. & Walker, J. R. (1995). Mutations in *Escherichia coli* dnaA which suppress a dnaX(Ts) polymerization mutation and are dominant when located in the chromosomal allele and recessive on plasmids. *J. Bacteriol.* **177**, 705–715.
35. Wang, R. F. & Kushner, S. R. (1991). Construction of versatile low-copy-number vectors for cloning, sequencing and gene expression in *Escherichia coli*. *Gene*, **100**, 195–199.
36. Link, A. J., Phillips, D. & Church, G. M. (1997). Methods for generating precise deletions and insertions in the genome of wild-type *Escherichia coli*: application to open reading frame characterization. *J. Bacteriol.* **179**, 6228–6237.
37. Ohta, T., Sutton, M. D., Guzzo, A., Cole, S., Ferentz, A. E. & Walker, G. C. (1999). Mutations affecting the ability of the *Escherichia coli* UmuD′ protein to participate in SOS mutagenesis. *J. Bacteriol.* **181**, 177–185.
38. Bunting, K. A., Roe, S. M. & Pearl, L. H. (2003). Structural basis for recruitment of translesion DNA polymerase Pol IV/DinB to the beta-clamp. *EMBO J.* **22**, 5883–5892.
39. Pritchard, A. E., Dallmann, H. G., Glover, B. P. & McHenry, C. S. (2000). A novel assembly mechanism for the DNA polymerase III holoenzyme DnaX complex: association of deltadelta′ with DnaX(4) forms DnaX(3)deltadelta′. *EMBO J.* **19**, 6536–6545.
40. Lusetti, S. L., Hobbs, M. D., Stohl, E. A., Chitteni-Pattu, S., Inman, R. B., Seifert, H. S. & Cox, M. M. (2006). The RecF protein antagonizes RecX function via direct interaction. *Mol. Cell*, **21**, 41–50.
41. Cohen, A. E., Ellis, P. J., Miller, M. D., Deacon, A. M. & Phizackerley, R. P. (2002). An automated system to mount cryo-cooled protein crystals on a synchrotron beamline, using compact sample cassettes and a small-scale robot. *J. Appl. Crystallogr.* **35**, 720–726.
42. McPhillips, T. M., McPhillips, S. E., Chiu, H. J., Cohen, A. E., Deacon, A. M., Ellis, P. J. *et al.* (2002). Blu-Ice and the Distributed Control System: software for data acquisition and instrument control at macromolecular crystallography beamlines. *J. Synchrotron Radiat.* **9**, 401–406.
43. Otwinoski, Z. & Minor, W. (1997). Processing of X-ray diffraction data collected in oscillation mode. *Methods Enzymol.* **276**, 307–326.
44. Vagin, A. & Teplyakov, A. (1997). MOLREP: an automated program for molecular replacement. *J. Appl. Crystallogr.* **30**, 1022–1025.
45. Collaborative Computational Project, Number 4 (1994). *Acta Crystallogr., Sect. D: Biol. Crystallogr.* **50**, 760–763.
46. Murshudov, G. N., Vagin, A. A., Lebedev, A., Wilson, K. S. & Dodson, E. J. (1999). Efficient anisotropic refinement of macromolecular structures using FFT. *Acta Crystallogr., Sect. D: Biol. Crystallogr.* **55**, 247–255.
47. Murshudov, G. N., Vagin, A. A. & Dodson, E. J. (1997). Refinement of macromolecular structures by the maximum-likelihood method. *Acta Crystallogr., Sect. D: Biol. Crystallogr.* **53**, 240–255.

48. Emsley, P. & Cowtan, K. (2004). Coot: model-building tools for molecular graphics. *Acta Crystallogr., Sect. D: Biol. Crystallogr.* **60**, 2126–2132.
49. Miller, J. H. (1999). A Short Course in Bacterial Genetics: A Laboratory Manual Handbook for *Escherichia coli* and Related Bacteria. Cold Spring Harbor Laboratory Press, Cold Spring Harbor, NY.
50. Sambrook, J., Fritsch, E. F. & Maniatis, T. (1989). *Molecular Cloning: A Laboratory Manual*, 3rd edit Cold Spring Harbor Laboratory Press, Cold Spring Harbor, NY.